
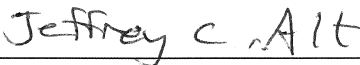
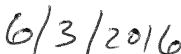


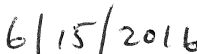

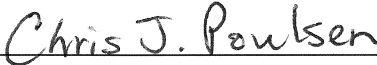



David J. Levine

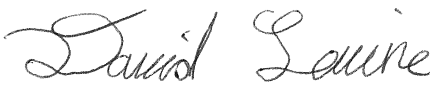
**Hydrothermal Alteration in the Subsurface  
of an Oceanic Ultramafic Hosted Hydrothermal System  
(as Preserved in Ligurian Ophiolites, Italy)**

submitted in partial fulfillment of the requirements for the degree of  
**Master of Science in Earth and Environmental Sciences**  
Department of Earth and Environmental Sciences  
The University of Michigan

 Signature	Accepted by:  Name	 Date
 Signature	 Name	 Date
 Department Chair Signature	 Name	 Date

I hereby grant the University of Michigan, its heirs and assigns, the non-exclusive right to reproduce and distribute single copies of my thesis, in whole or in part, in any format. I represent and warrant to the University of Michigan that the thesis is an original work, does not infringe or violate any rights of others, and that I make these grants as the sole owner of the rights to my thesis. I understand that I will not receive royalties for any reproduction of this thesis.

- Permission granted.  
 Permission granted to copy after: \_\_\_\_\_  
 Permission declined.



Author Signature



**Hydrothermal Alteration in the Subsurface  
of an Oceanic Ultramafic-Hosted Hydrothermal System  
(as Preserved in Ligurian Ophiolites, Italy)**

David J. Levine

Department of Earth and Environmental Sciences

University of Michigan, Ann Arbor

June 2016

## **Abstract**

Geochemistry and petrology of serpentinized peridotites from the Ligurian Ophiolites, Italy were analyzed to investigate alteration processes in the subsurface of an ocean detachment fault. Three dominant processes were identified: 1) Serpentinization of peridotites preserves a primary seafloor hydrothermal signature, with elevated light rare earth element (LREE) contents and  $\delta^{34}\text{S}$  values; 2) Talc alteration + mineralization associated with a fault and high temperature fluids ( $\sim 350^\circ\text{C}$ ) that resulted in silica metasomatism, elevated LREE + metal contents, and deposition of a massive sulfide deposit; and 3) Carbonate replacement + precipitation related to low-temperature hydrothermal fluids ( $20^\circ\text{C} - 125^\circ\text{C}$ ) that were focused in the fault zone resulting in intense metasomatism: including enrichments of REE, metals, silica and calcium. The alteration in this on-land proxy to ocean crust constrains fluid pathways that are poorly understood on the seafloor because of difficulties sampling on the seafloor. In particular, results show that normal faults that cut the detachment surface act as conduits to transport fluids from deeper in the subsurface to the ocean floor. These results further understanding of the controls on fluid pathways and processes such as volcanogenic massive sulfide (VMS) formation and carbon sequestration in ultramafic- hosted hydrothermal systems.

## Table of Contents

<b>Introduction</b>	4
<b>Geologic Setting</b>	6
<b>Geology of Sampling Site</b>	8
<b>Methods</b>	9
<b>Sample Descriptions</b>	10
<i>Background Serpentinites</i>	10
<i>Carbonate-Veined Serpentinites</i>	11
<i>Mineralized Talc Altered Serpentinites</i>	11
<i>Serpentinite Breccia</i>	12
<i>Fault Zone Breccia</i>	12
<i>Basalts</i>	13
<b>Results</b>	13
<i>Major Elements and Metals</i>	13
<i>Rare Earth Elements (REE)</i>	14
<i>Trace Elements</i>	15
<i>Electron Microprobe Analysis (EPMA)</i>	16
<i>Bulk Rock Carbon Geochemistry</i>	17
<i>Carbon and Oxygen Isotope Compositions</i>	17
<i>Temperature of Carbonate Precipitation</i>	18
<i>Sulfur Isotope Compositions</i>	18
<b>Discussion</b>	19
<i>Serpentinization</i>	19
<i>Talc Alteration</i>	22

<i>Carbonate Formation</i>	23
<i>Fault Rocks</i>	25
<b>Conclusions</b>	28
<b>References</b>	30
<b>Figures</b>	37
<b>Tables</b>	55

## **Introduction**

Limited magma supply at slow and ultra-slow ocean spreading ridges leads to local extension resulting in shallow detachment faults that exhume mantle peridotites on the seafloor (Escartin, 2011). Exhumed peridotites are variably metamorphosed and hydrated as they are exposed to fluids by detachment faulting where they undergo serpentinization. There can be significant variability in rocks that have undergone serpentinization reactions, but common mineral products are serpentine (chrysotile, lizardite and antigorite), brucite, talc, and magnetite with hydrogen and methane production (Bach et al., 2004). Serpentinized ocean crust is abundant and believed to comprise up to 25% of basement rocks at slow-spreading ridges (Cannat et al., 2010). Serpentinites are rocks primarily composed of any of the three serpentine polymorphs which play a vital part in important seafloor processes such as chemical exchange between the crust and seawater along with supporting chemosynthetic microbial communities in the ocean subsurface (Shrenk et al., 2013). Serpentinites can also sequester natural CO<sub>2</sub> which makes them an important component of ocean basement (Keleman et al., 2011).

Detachment surfaces are marked on the seafloor by corrugated, dome-like structures called oceanic-core complexes (OCCs). These seafloor structures have been identified at mainly slow-spreading ridges, while occasionally appearing at intermediate-spreading ridges (Blackman et al., 2009). They are composed of different amounts of basalt, gabbro and peridotites that are variably serpentinized (Blackman et al., 2009). OCCs can be readily identified on the seafloor by their contrasting morphology with surrounding rocks and positive gravity anomalies (Blackman et al., 2009). These seafloor structures are of particular interest because they contain ultramafic-

hosted hydrothermal systems that differ from more common basalt-hosted systems (Lowell, 2010).

When these hydrothermal systems are active, they transport hot fluids ( $>350^{\circ}\text{C}$ ) to the surface where black smokers vent and massive sulfides are precipitated. These processes have been recognized at various OCCs with notable occurrences at the Rainbow massif, Logachev hydrothermal field and Semenev Ore District, all on the Mid-Atlantic Ridge (Andreani et al., 2014, Petersen et al., 2000, Pertsev et al., 2012). The temperature and heat flux at these seafloor discharge zones indicate that serpentinization alone cannot provide the necessary heat, and that a magmatic heat source at depth provides an important contribution. (German and Lin, 2004; Andreani et al., 2014). As hot, acidic hydrothermal fluids pass through these ultramafic rocks they can easily transport metals, but as the fluids conductively cool ( $<100^{\circ}\text{C}$ ) they become more alkaline and are able to precipitate carbonate minerals that can replace existing rock assemblages (Foustoukos et al., 2008, Schwarzenbach et al., 2013). Examples of these processes have been observed at the Lost City and Ghost City fossil hydrothermal systems (Fruh-Green et al., 2003, Lartaud et al., 2011, Andreani et al., 2014). These deposits are located on top of serpentinized basement rock in the near subsurface of OCCs where upwelling hydrothermal fluids are focused and interaction with seawater takes place.

Past studies have particularly focused on the exposed detachment faults themselves and on the hydrothermal alteration found at these OCCs to better understand fluid penetration, metamorphism and serpentinization that is associated with the uplift and exposure of these mantle rocks (Schmidt et al., 2007; McCaig et al., 2010; Smith et al., 2014)). These areas are hard to access, but sampling has been done on the seafloor and near subsurface by submersible, dredging and rock-drill. Vents atop the exposed detachment fault surfaces have been suggested

to be fed by faults at a high angle to the detachment, but these have not yet been directly sampled on the seafloor (Figure 1; Andreani et al., 2014). Seismic evidence of fault conduits and pathways that can transport fluids at depth has been observed, but direct sampling of these faults for high resolution analysis has not yet been done (Andersen et al., 2015). Directly sampling the subsurface below these detachment faults would allow for better understanding of hydrothermal flow paths and the distribution of alteration and mineralization that is currently weakly constrained (Escartin, 2011).

In the Northern Apennines, basalt, peridotite and serpentinite outcrop, preserving the ancient Ligurian Tethys seafloor. Mantle peridotites were exposed to the seafloor by detachment faulting prior to the extrusion of basalts and deposition of sediments during extension of this sea (Piccardo et al., 2002). These peridotites preserve a geochemical signature of depleted mantle lithosphere (Rampone, 1996). In an area just north of the village of Reppia in the Internal Ligurides (IL), the rocks preserve an oceanic normal fault that cuts the detachment surface at a high angle. This fault acted as a fluid conduit and allowed for the focusing of hydrothermal fluids that altered the surrounding rocks and formed a massive sulfide deposit on the ancient ocean floor. These exposed ophiolites offer a unique opportunity to study the subsurface of an ultramafic hosted hydrothermal system and provide insight to what cannot be directly sampled on the modern seafloor.

## **Geologic Setting of the Northern Apennine Ophiolites**

Ophiolites in the Northern Apennines of Italy are linked to the Ligurian Tethys Ocean that was formed by the separation of the Adria Plate from the European Plate in the middle Jurassic (Lemoine., 1987). This rifting event coincided in timing with the opening of the Atlantic



Ocean and can be linked to the passive extension of the Europe-Adria lithosphere (Piccardo, 2008). It is believed that the extension is related to an oblique detachment fault (Lemoine et al., 1987) caused by three main processes: thinning of continental crust, the upwelling of subcontinental lithospheric mantle and the intrusion of small gabbroic bodies in the upper mantle (Figure 2.A).

These processes resulted in the initial opening of a small ocean basin that was exposing sub-continental lithosphere consisting of peridotite and MORB gabbros before being covered by an outflow of MORB lavas and buried by pelagic sediments (Figure 2.B; Garuti et al., 2008; Piccardo, 2008). This stratigraphic succession is expected in classical oceanic crust although sheeted dykes are absent. Sheeted dykes have commonly been a necessary feature when describing ocean crust, but recent work has shown that they can be absent in OCCs (Escartin, 2011). Besides this difference, the presence of MORB basalts and the striking similarity of the Apenninic Ophiolites to ocean crust allow them to be described as such. In the Late Cretaceous, the divergence occurring in the Ligurian Tethys shifted to a convergent regime that emplaced pieces of this ocean lithosphere on land as thrust units in the Alps and Apennines (Figure 2.C; Muntener and Piccardo, 2003). Ophiolites emplaced in northern Italy were subject to different types of tectonic emplacement which resulted in different metamorphic facies to the west and east. The Western Alps show evidence of high pressure, low temperature metamorphism preserved as eclogite- and blueschist-facies while the Northern Apennines show only minor metamorphism preserved as prehnite-pumpellyite facies (Figure 3; Garuti et al., 2008). Ophiolites of the Northern Apennines retain seafloor alteration effects and serve as a proxy to study seafloor hydrothermal processes associated with ultramafic rocks (Scambelluri et al., 1997).

## Geology of Sampling Site

The sampling site is located in an area just north of Reppia, Italy which is located in the Internal Ligurides of the Northern Apennines. Samples were taken from a location where outcropping peridotites are overlain by basalts and sediments, and offset by a high angle normal fault that cuts the detachment surface. The fault zone is approximately 5–10 m wide and is oriented at a high angle to the paleo-seafloor with outcrops extending over 100 meters (Figure 4). The fault juxtaposes a footwall of serpentinite and serpentinite breccia on the west against a sequence of pillow basalts in the hanging wall to the east. The fault ends upward in mineralized and hydrothermally altered pillow lavas that overlie the serpentinite that are continuous with the lavas adjacent to the fault on the east (Figure 4). The pillows are overlain by pelagic chert and limestone. Serpentinite underlying pillow basalts on the down dropped eastern side is not exposed, so the fault could have an offset of 50 m up to 150-200 m. The fault zone itself comprises mainly of carbonate with minor quartz, chlorite, sulfides and chrome spinel. Also present are rare decimeter scale blocks of recrystallized pelagic limestone. Carbonate-cemented serpentinite breccia extends for 45 m away from the fault on the west, with a 5 m wide lens of sheared and chloritized basalt adjacent to the fault (Figure 4). At 60 m away from the fault is a 2-5 m thick zone of talc + sulfide veins and variably talc-altered serpentinite (Figure 4), similar to talc altered shear zones that are exposed in serpentinite from deeper below the paleo-seafloor ~500 m to the SE. The serpentinite host to this talc + sulfide veining is mainly massive, macroscopically unveined serpentinite, but ranges to serpentinite variably veined by carbonate that locally comprises up to ~25% of the rock by volume.

## Methods

Petrography and mineralogy of the samples were analyzed in 21 polished thin sections. Minerals were identified by X-Ray Diffraction using a Rigaku Ultima IV X-Ray Diffractometer.

Samples for bulk rock chemistry were trimmed with a rock saw, crushed in a steel jaw crusher and powdered using a tungsten carbide shatter box. Bulk rock XRF and ICP-MS major and trace element analyses were made at the Peter Hooper Geochemistry Lab of Washington State University. The precision for XRF analysis was within 3.3%. A CAMECA SX-100 Electron Probe Microanalyzer (EPMA) was used to measure Ca, Fe, Mg, Mn, and Sr oxide concentrations of carbonates in thin sections.

Carbon and oxygen stable isotope analyses were performed using routine techniques at the University of Michigan. Bulk rock carbon contents and  $\delta^{13}\text{C}$  values were measured using a Finnegan MAT Delta S triple-collector gas source mass spectrometer coupled to a Costech Element Analyzer. Thin section chips were spot drilled for carbonate mineral separates that were analyzed for  $\delta^{18}\text{O}$  and  $\delta^{13}\text{C}$  using a Finnegan MAT 251 triple-collector gas source mass spectrometer coupled to a Kiel automated preparation device.

Sulfur was analyzed in 3 samples. 9 g of whole rock powder was reacted with a series of acids under N<sub>2</sub> atmosphere, following the procedure of Rice et al. (1993) to extract AVS (Acid-volatile, or monosulfide sulfur), CRS (chrome-reduced sulfide, or pyrite sulfur) and Sulfate-sulfur. Sulfur was precipitated as Ag<sub>2</sub>S and the amounts of sulfate-, monosulfide- and disulfide-sulfur were determined gravimetrically, and the relative precision of the sulfur contents was within 3%.

Sulfur isotope ratio measurements were carried out on the bulk rock sulfur and a chalcopyrite separate from a sulfide boulder from a fault zone in serpentinite at ~300 m below

the paleo seafloor, 1 km to the SE of the field site. Sulfur isotopes were analyzed using an elemental analyzer coupled to a Thermo Delta XP mass spectrometer at the USGS stable isotope laboratory in Denver, Colorado. Standard deviation of the  $\delta^{34}\text{S}$  of standards was  $<\pm 0.4\%$ .

## **Sample Descriptions**

Samples were collected along a 60 m transect across the high-angle fault along road cuts sub-parallel and ~20 m below the detachment surface. Multiple samples were taken of each lithology.

### *Background Serpentinites*

Two background serpentinites that show no talc or carbonate alteration were collected from locations nearby the field site. The first sample was collected at a road cut 200 m east of the field site, while the second was collected 100 m south of the first one from deeper in the subsurface. These two serpentine samples are indicative of the background composition of the serpentinites before they were intensely altered by different composition hydrothermal fluids. The olivine in these samples is completely altered to serpentine while minor relict pyroxene remains (Figure 5.A). Previous work has shown the serpentine minerals present in these serpentinites are chrysotile and lizardite. (Scambelluri et al., 1997). Some of the pyroxenes display a “bastite” texture in their cores with unaltered rims. The rocks display a well-developed, equant mesh texture (Roumejon and Cannat, 2014) and contains approximately 15% magnetite (Figure 5.A). The magnetite grains are no larger than 50  $\mu\text{m}$  and fill cracks produced during serpentinization. The two background samples are both  $> 90\%$  serpentinized, but one sample is more serpentinized and lacks unaltered relict pyroxenes. Trace chrome-spinel are present as 100

$\mu\text{m}$  to  $750 \mu\text{m}$  irregular grains (Figure 5.B) and trace chlorite is also present, appearing as  $\sim 0.5$  mm patches.

### *Carbonate-Veined Serpentinites*

The samples with the least amount of post-serpentinization alteration are carbonate-veined serpentinites that contain serpentine with minor talc and varying amounts of calcite veins. These three samples were gathered from between 60–45 m west of the fault zone. The serpentine consists of mostly equant, mesh texture but in some sections of the thin sections a stretched ribbon texture is present. In these altered serpentinites, disseminated talc replaces the pyroxene phenocrysts and forms replacement veins that are  $50\text{--}350 \mu\text{m}$  wide (Figure 5.C+D). Larger, twinned calcite veins with a thickness of 1-4 mm cut across the serpentine and relict pyroxenes (Figure 5.C+D). These veins have jagged edges where calcite replaces the surrounding serpentine and pyroxenes in zones  $\sim 10\text{--}40 \mu\text{m}$  wide. Minor amphibole is present in the core of bastite pseudomorphs of pyroxene. The magnetite is very fine-grained ( $<50 \mu\text{m}$  across), represents less than  $\sim 4\%$  of the sample and fills in cracks similar to the background serpentinite. Trace chrome–spinel are also present, similar in morphology to what is in the background serpentinites.

### *Mineralized Talc Altered Serpentinites*

Three samples were collected in a 2.5 m wide zone highly altered to talc and associated with sulfide minerals in the outcrop of calcite-veined serpentinite, 60–55 m to the west of the fault zone. One sample is 100% replaced by talc with the second being 90% replaced by talc (Figure 5.E). In the less altered sample, talc is replacing serpentinite fragments and relict pyroxenes. The third sample contains 70% sulfide minerals which are composed of irregular,

subhedral pyrite and chalcopyrite, both partly weathered to oxides (Figure 5.F). The rest of the sample consists of disseminated talc replacing serpentinite fragments that are 30–475  $\mu\text{m}$  across.

### *Serpentinite Breccia*

Serpentine breccias occur for 45 m to the west of the fault zone. Three breccia samples are calcite matrix supported and composed of 1–9 mm angular clasts of serpentinite. The amount of serpentinite clasts varies from 20% to 40%. The serpentinite clasts are cut by  $\sim 200$   $\mu\text{m}$  calcite veins or by talc veins  $\sim 100$   $\mu\text{m}$  thick that partly replace the host serpentinite clast. The serpentinite clasts are also in some places completely replaced by talc or calcite (Figure 6.A+B). The clasts are cemented by a matrix composed of clear, subhedral twinned calcite crystals up to 0.5 mm in size.

### *Fault Zone Breccia*

Four samples collected from the fault zone consist mainly of dolomite with minor calcite and quartz, patches and clasts of serpentine and chlorite, with traces of sulfide minerals and chrome-spinel. The carbonates appear as interlocked “feathery” grains that are up to 1 mm long or as 5–200  $\mu\text{m}$  euhedral to subhedral rhombohedral crystals (Figure 6.C+D). There is no distinction in textures for the calcite and dolomite. Minor quartz appears throughout the samples as 20  $\mu\text{m}$  to 3 mm anhedral to subhedral grains intergrown with the carbonates. Quartz locally contains inclusions of chlorite and serpentine, and has a “fibrous” internal texture, suggesting formation by replacement of serpentinite. Sulfide minerals consists of pyrite  $\pm$  chalcopyrite  $\pm$  sphalerite  $\pm$  pyrrhotite in 25  $\mu\text{m}$  to 400  $\mu\text{m}$  grains and aggregates (Figure 6.E). Trace chrome-spinel are present and similar to those in host serpentinite (Figure 6.F). Altered serpentine clasts

scattered in these samples vary from 3 mm to 3.5 mm and are partly replaced by calcite and dolomite. Chlorite occurs as local patches and clasts, up to several hundred micrometers in size.

One fault rock sample (70914-2) is clearly a breccia, consisting of rounded clasts, hundreds of micrometers up to several millimeters across and composed of intergrown carbonates and quartz, with local 10-100  $\mu\text{m}$  laths of hematite (Figure 7.A). These clasts are cemented by fine grained (4-100  $\mu\text{m}$ ) euhedral dolomite and granular quartz, with the dolomite rimmed by Fe-oxyhydroxide weathering products.

### *Basalts*

Basalts preserve a primary basalt texture but are altered to quartz and albite with minor chlorite and titanite (Figure 7.B). Quartz varies from 50  $\mu\text{m}$  to 150  $\mu\text{m}$  grains that fill veins cutting across albite.

At the top of the fault, the serpentinites are covered by basalts. These basalts are completely altered to pyrite and quartz with minor chalcopyrite, and associated with illite, chlorite and titanite. Sulfides and quartz are the only identifiable minerals in thin section (Figure 7.C+D). The sulfides range from 20  $\mu\text{m}$  to 300  $\mu\text{m}$  while the quartz ranges from 5  $\mu\text{m}$  to 500  $\mu\text{m}$ .

On both sides of the fault zone, lenses of basalts have been sheared and altered completely to chlorite with minor titanite (Figure 7.E).

## **Results**

### *Major Elements and Metals*

Whole-rock major element compositions were analyzed on multiple samples of each lithology (Figure 8). Major element compositions normalized to volatile-free compositions were used (Table 1) because loss on ignition was substantial for some samples and ranged from 4–34 wt% depending on the amount of carbonate in the sample. Only the background samples plot in the field of harzburgite – lherzolite oceanic mantle as defined by Bodinier and Godard (2013) for  $\text{Al}_2\text{O}_3/\text{SiO}_2 + \text{MgO}/\text{SiO}_2$ . Background samples both have 8.6 wt % FeO while veined serpentinite and fault zone rocks are elevated in FeO (>10 wt%) and serpentinite breccias have low FeO (<6.9 wt %). Background samples also have the greatest MgO/SiO<sub>2</sub> ratio, which decreases with the veined serpentinite, followed by the serpentinite breccias, while the smallest MgO/SiO<sub>2</sub> ratio is found in the talc altered serpentinite and fault zone breccias that contain elevated levels of SiO<sub>2</sub> or CaO. CaO contents vary from 0.01–0.61 wt%, with the highest concentrations found in the fault zone breccias which consist dominantly of carbonate minerals. The lowest concentrations of CaO are found in the talc altered serpentinites, which contain almost zero CaO, but they contain the highest SiO<sub>2</sub> concentrations of >57 wt%.

Cu has the largest spread of metal concentrations, followed by Ni and Zn, with Cr having the smallest spread (Figure 9). The two zones of sulfide mineralization (mainly iron and copper sulfides) are associated with a massive sulfide deposit (data not plotted on Figure 9) and a zone of sulfide mineralization found associated with the talc-altered and veined serpentinites, which both have elevated Cu concentrations.

### *Rare Earth Elements (REE)*

Chondrite-normalized whole-rock REE patterns of all the samples are shown in Figure 10 together with the composition of depleted peridotites from N-MORB ophiolites of the Internal



Ligurides (IL), Italy (McDonough and Sun, 1995; Rampone et al., 1996). Background serpentinites are similar in composition to the depleted peridotites, although they are elevated in LREE (Figure 10.A). Other samples all show varying REE patterns, but samples of the same lithology all display similar patterns to each other or to nearby samples of different lithologies.

The two talc altered serpentinites have a flat REE pattern with an enrichment in LREE and a strong depletion in Eu (Figure 10.B). The two samples vary in the amount of Eu depletion, but range from 5x to 10x less than the other REE concentrations in those rocks.

The three carbonate-veined serpentinites have REE patterns that are generally like those of the talc altered serpentinites (Figure 10.C). Two samples have negative Eu anomalies, similar to what is observed in the talc altered serpentinites. The least veined carbonate serpentinite (sample 26-3) has no Eu anomaly and a REE pattern similar to the background serpentinites.

The three serpentinite breccia samples have flat REE patterns enriched in LREE relative to the IL peridotite with two samples showing a positive Eu anomaly, similar to what is found in venting hydrothermal fluids on the seafloor (Douville et al., 2002; Figure 10.D). The third sample has a negative Eu anomaly, similar to the talc-altered samples. These three samples are all petrographically similar, but the two samples displaying the positive Eu anomaly contain smaller clasts that are more extensively replaced by carbonate. The breccia with the negative Eu anomaly contains larger clasts with greater amounts of talc than the other samples (sample 26-8).

The two fault rock samples show extreme enrichment in total REEs, with an overall LREE enrichment pattern and no Eu anomaly (Figure 10.E).

### *Trace Elements*

Major elements and REE show the greatest variations, but other trace elements also show significant trends. Concentrations of Sc, V and Ga show variation among samples, but it is not systematic. Elements that do show systematic variations are Sr and Y. Background rocks show Sr and Y concentrations similar to bulk earth composition (Figure 11), while the rest of the serpentinites were normalized to background compositions to highlight differences (Figure 12). Variations in Sr are significant, but Y concentrations are <15 ppm and could vary from analytical uncertainty.

Talc altered rocks show a strong depletion in Sr. The carbonate-veined serpentinites show a strong enrichment in Sr with the serpentinite breccias having an even stronger Sr enrichment. The fault zone breccia samples show the greatest enrichment in Sr. This is a systematic trend, where there is more Sr in rocks containing more carbonate.

### *Electron Microprobe Analysis (EMPA)*

Carbonates were analyzed to identify any chemical differences between the different textures (Table 2). Calcite has low MgCO<sub>3</sub> and FeCO<sub>3</sub> (0.34 to 7.5 wt%) contents whereas dolomites are iron-rich and contain higher amounts of MgCO<sub>3</sub> and FeCO<sub>3</sub> (11.2 to 31 wt%; Figure 13). Sr and Mn concentrations were measured as well but showed no consistent variation. Calcite was found in all samples while the iron-rich dolomite was only found in the fault-rocks where it is the primary carbonate mineral.

In fault rock 61598-1, “light” (Figure 6.C) and “dark” (Figure 6.C) feathery carbonates are mainly iron-dolomites, with only minor local calcite. Carbonates in fault rock sample 26-14 vary from feathery texture (Figure 6.D) to well-formed euhedral rhombs (Figure 6.D). These different textures did not correspond to differences in compositions, with both being mainly iron-

dolomite with minor local calcite. In the serpentinite breccia, sparry calcite cement composes the matrix (Figure 6.A) as well as fine-grained calcite cement that replaces serpentine (Figure 6.B). The different textures are both low in Mg and Fe with no differences in composition. In the carbonate veined serpentinites, 1–4 mm thick carbonate veins (Figure 5.C) and the zones of carbonate replacement (Figure 5.D) of serpentine along the veins are both low in Mg and Fe with no differences in composition.

### *Bulk Rock Carbon Geochemistry*

8 samples with visible carbonate in thin section (veined, breccia and fault zone samples) and 2 background samples were analyzed for bulk rock total carbon (TC) contents and their  $\delta^{13}\text{C}$  isotopic signature (Table 3). Samples in the fault zone contain the most carbon (up to 10.9 wt%) while the least altered background serpentinites, farthest away from the fault zone, contained the smallest amount of carbon (between 0.03 and 0.04 wt%).

$\delta^{13}\text{C}$  values of the bulk rock vary from -9.2 to -6.7 ‰ VPDB in the background rocks, -4.8 to -0.2 ‰ in the carbonate veined serpentinites, 0.68 to 1.4 ‰ in the serpentinite breccias and -2.3 to -1.8 ‰ in the fault zone breccia.

### *Carbon and Oxygen Isotope Compositions*

$\delta^{13}\text{C}$  values for the different carbonate separates are constrained between -1.5 and 2.4 ‰ VPDB while  $\delta^{18}\text{O}$  values fall between 19.6–29.6 ‰ VSMOW (Table 4).

Each distinct lithology that these carbonate measurements were taken from form even tighter clusters when  $\delta^{18}\text{O}$  and  $\delta^{13}\text{C}$  values are plotted (Figure 10).  $\delta^{13}\text{C}$  for carbonate veins in the carbonate-veined serpentinites fall between -0.76 and 0.98 ‰ VPDB with  $\delta^{18}\text{O}$  values between

19.7–26.6 ‰ VSMOW. The  $\delta^{13}\text{C}$  values for the carbonate matrix of the serpentinite breccias vary from 0.9–2.9 ‰ VPDB with  $\delta^{18}\text{O}$  values ranging from 19.6–29.6. Lastly,  $\delta^{13}\text{C}$  values for the fault-zone breccia fall between -1.5 and -0.8 ‰ VPDB with  $\delta^{18}\text{O}$  values between 19.8–20.94 ‰ VSMOW. There are no distinct isotope variations between the calcite and dolomite or vein and matrix.

### *Temperature of carbonate precipitation*

Oxygen isotope compositions were used to calculate carbonate-precipitation temperatures, assuming equilibrium between carbonate minerals and seawater ( $\delta^{18}\text{O}_{\text{seawater}} = 0\text{‰}$ ) by using the calcite-water fractionation factor from Friedman and O’Neil (1977). Calculated temperatures of calcite fall between 20–80°C (Table 4), with no distinction in temperature between matrix and veins. Temperatures calculated from the fault rocks, have the potential to be ~22°C warmer (Table 4), due to the fact that they contain mostly dolomite. For fault rocks, the dolomite-water fractionation factor from Vasconcelos et al., (2005) was used assuming a  $\delta^{18}\text{O}_{\text{seawater}} = 0\text{‰}$ . Calculated temperatures of formation for the fault rocks if they contained all dolomite fall between 91–102°C. In the samples there is some minor calcite, which would lower these temperatures slightly.

If carbonates formed from hydrothermal fluids having slightly higher oxygen values where  $\delta^{18}\text{O} = +2\text{‰}$  (Ribeiro de Costa et al., 2008), calculated temperatures for the calcite in all of the rocks would be approximately 29–97 °C, while fault rocks would have formed at 110–123°C (Table 4).

### *Sulfur Isotope Compositions*

Serpentinites contain varying amounts of sulfur (313–1155 ppm) and have different  $\delta^{34}\text{S}$  signatures (Table 5). Sulfur in the carbonate-veined serpentinite is dominated by AVS sulfide, with CRS sulfide being the dominant sulfur species in the serpentinite breccia and background serpentinite samples.  $\text{SO}_4/\Sigma\text{S}$  for the different samples ranges from 0.03–0.33.  $\delta^{34}\text{S}$  values for sulfide in the veined serpentinite and serpentinite breccia are negative and vary from -1.4 to -4.1‰ and -13.4 to -17.6‰ respectively.  $\delta^{34}\text{S}$  of sulfide in the background sample ranges from 3.9 to 5.2‰ while the chalcopyrite from the deep portion of the fault has a value of 5.7‰.

## Discussion

Peridotites at Reppia are intensely serpentinized, but preserve a primary seafloor signature with no influence from meteoric waters. Positive  $\delta^{18}\text{O}$  and relatively high  $\delta\text{D}$  values of serpentinites provide evidence for an ocean floor environment during serpentinization (Barret and Friedrichsen, 1989).

### *Serpentinization*

The composition of the background, “least altered” serpentinites is important for understanding the processes of serpentinization as well as the subsequent reaction pathways that the serpentinites have gone through. The least altered rocks all show high degrees of serpentinization, which is commonly the case for abyssal peridotites (Dick et al., 1984). Serpentinization can erase magmatic signatures in the compositions of the peridotites, and bulk rock analysis is generally not useful for understanding pre-serpentinization processes (Niu, 2004).

Figure 8 displays the bulk rock chemical compositions of Reppia samples plotted in  $\text{MgO}/\text{SiO}_2\text{-Al}_2\text{O}_3/\text{SiO}_2$  space along with the ‘terrestrial array’ line (Jagoutz et al., 1979; Hart and

Zindler, 1986). The background serpentinites plot just below the terrestrial array line with compositions of 0.88 and 0.97 MgO/SiO<sub>2</sub>. These values are comparable to the decrease of the MgO/SiO<sub>2</sub> ratio by  $5.1 \pm 6.1\%$  measured in a compilation of data for seafloor serpentinites (Malvoisin, 2015). The decrease of the MgO/SiO<sub>2</sub> ratio appears to be related to the scarcity of brucite in heavily serpentinized peridotites (Bach et al., 2004). There are two mechanisms that can together cause the decrease of the MgO/SiO<sub>2</sub> ratio and shortage of brucite: 1) Mg loss through brucite dissolution (Snow & Dick, 1995) and 2) SiO<sub>2</sub> gain through the reaction with high aSiO<sub>2</sub> fluids to form serpentinite with or without brucite as a reaction intermediate (Beard et al., 2009; Frost et al., 2013). These two mechanisms can separately or collectively cause the decrease in MgO/SiO<sub>2</sub> ratios in the serpentinites.

REE patterns of background serpentinites normalized to CI chondrite compositions are plotted along with peridotites from the Internal Ligurides (Rampone, 1996) that represent a depleted mantle composition (Figure 10.A). Middle and HREE contents of serpentinite and fresh peridotite are similar, but the serpentinites are enriched in LREE, consistent with interaction with LREE-enriched hydrothermal fluids (Figure 10.A).

Sulfur isotopes provide a useful tracer that can distinguish the effects of hydrothermal fluids on peridotites from those of cooler seawater serpentinization reactions (Figure 15; Alt et al., 2013).  $\delta^{34}\text{S}$  values of sulfide in the background serpentinite range from 3.9 to 5.2‰ while the chalcopyrite from deeper portions of the fault has a value of 5.7‰. Compared to mantle rocks, ( $\delta^{34}\text{S} = 0\text{‰}$ ) sulfide minerals from high-T UM hydrothermal sulfide deposits have elevated  $\delta^{34}\text{S}$  values (mean  $\approx +5\text{‰}$ ; Rouxel et al., 2004; Peters et al., 2010), reflecting a hydrothermal sulfide component in hydrothermal fluids.  $\delta^{34}\text{S}$  of sulfide minerals in VMS deposits at Reppia have an average value between 3.1 and 5.4‰ (Garuti et al., 2009). Combined with the LREE enrichment,

this demonstrates that the background serpentinites underwent hydrothermal alteration by high-T hydrothermal fluids while on or beneath the seafloor.

Whole rock  $\delta^{18}\text{O}$  measurements of serpentinites can be used to get a rough estimate of temperatures of serpentinization using the water-rock calculation of Taylor (1977). Measured  $\delta^{18}\text{O}$  values of the rock can be used with assumed  $\delta^{18}\text{O}$  values of the fluid to solve for temperature and water/rock ratio. The  $\delta^{18}\text{O}$  values from Rosli et al., (1991) for serpentinites in the Reppia area vary from 4.3 to 6.1‰. Assuming equilibrium with seawater ( $\delta^{18}\text{O} = 0\text{‰}$ ), temperatures were 150°C to 400°C. If the fluid was instead an  $^{18}\text{O}$ -enriched hydrothermal fluid ( $\delta^{18}\text{O} = +3\text{‰}$ ), temperatures would range from 200°C–400°C (Alt et al., 2007). At temperatures  $> 350^\circ\text{C}$  olivine is stable so little or no serpentinization occurs (Alt and Shanks, 2003). 350°C is therefore the likely maximum temperature of serpentinization. These hydrothermal temperatures are consistent with LREE enrichment and sulfur isotope data.

Serpentinization can occur during uplift along the detachment fault, and there is evidence for hydrothermal fluids along detachments so the hydrothermal signature could have formed at depth (McCaig, 2010). The fault rocks are associated with a zone of focused flow that deposited a seafloor sulfide deposit, which could also mean that the hydrothermal signature was from reactions the serpentinites were exposed to on the seafloor. Andreani et al., (2007) identified two main stages of serpentinization that occur as peridotite is exhumed by detachment faults by studying the progression of 4 veining episodes in drill core from the mid-Atlantic Ridge (V1–V4). V1–V3 occur at 3 to 8 km depths in closed, diffusive systems along the detachment fault where serpentinization temperatures range from around  $<200\text{--}350^\circ\text{C}$  (Hebert et al., 1990). V4 are generated closer to the surface where there is an open hydrothermal system in the shallow lithosphere ( $<2\text{ km}$ ) that corresponds to temperatures of  $<150\text{--}200^\circ\text{C}$  (Andreani et al., 2007).

Geochemical data provides evidence that these serpentinites were altered in one of these regimes, although it cannot be said for certain exactly which stage.

### *Talc Alteration*

Serpentinite altered to talc and associated with sulfide mineralization is found ~50 m west of the visible fault zone. Talc alteration is also found partly to completely replacing clasts in the serpentinite breccia and forming veins in the veined serpentinite. The observed talc alteration can be attributed to a metasomatic event that overprinted serpentinization and is associated with high temperature SiO<sub>2</sub>-rich hydrothermal fluids (Paulick, et al., 2006; Malvoisin, 2015).

With the exception of the fault rocks, the lowest MgO/SiO<sub>2</sub> ratios (<0.52) are found in talc altered serpentinites (Figure 8). These rocks contain serpentine that has been completely replaced by talc (90–100%) with associated sulfide mineralization. This most likely occurred through the addition of silica to serpentine (Mg<sub>3</sub>Si<sub>2</sub>O<sub>5</sub>(OH)<sub>4</sub>), to form talc (Mg<sub>3</sub>Si<sub>4</sub>O<sub>10</sub>(OH)<sub>2</sub>). Associated sulfide mineralization suggests hydrothermal fluids enriched in metals and silica (Seyfried et al, 2011). A source for the silica in these fluids has been suggested as gabbro at depth (Bach et al., 2004), which might also be the source for sulfides (Alt and Shanks, 2003) in these rocks.

The talc altered serpentinites have relatively flat REE patterns, with a strong depletion in Eu (Figure 10.B). Similar REE patterns occur in two of the veined serpentinites (Figure 10.C) as well as one serpentinite breccia sample (Figure 10.D), which all contain significant amounts of talc. LREE are enriched relative to the IL peridotites, while having a slightly depleted HREE signature. This enrichment of LREE is consistent with interaction with silica-rich hydrothermal fluids that formed the talc and enriched the serpentinites in sulfur.



Similar talc alteration of serpentine is observed in serpentinite from the Mid- Atlantic Ridge (Paulick et al., 2006). A first stage of serpentinization that contained disseminated pyrite with pyrite veins that correlated to elevated sulfur concentrations was followed by significant alteration to talc. The REE signature of the serpentinites show similarities to REE patterns of hydrothermal fluids measured at black smokers of UM-hosted hydrothermal systems, although the LREE and MREE vary greatly (Paulick, et al., 2006). The end-member compositions of these hot (350–400 °C), metal-rich fluids show LREE enrichment with a strong positive Eu anomaly (Figure 10). The mineralized talc altered rocks sampled by Paulick show similar LREE enrichment and the same negative Eu anomaly that is observed in the Reppia talc altered samples. The talc alteration clearly overprints serpentinization, on the seafloor and at Reppia, but the exact mechanism for generation of the REE patterns is not clear. Paulick et al., 2006 suggests that Eu may reside in a different phase than the other REE in the protolith and that upon talc alteration the Eu-bearing phase is destroyed while the other REE-bearing phase is stable.

The serpentinite breccia sampled closest to the talc alteration contains the most talc of the breccia samples, and has an almost identical REE pattern to the talc altered rocks.

### *Carbonates*

Carbonate formation is an important process that takes place in UM hosted hydrothermal systems as thermal supply diminishes and temperatures began to wane (Schwarzenbach et al., 2013). An indication of cooling in these systems is carbonate replacement of serpentinite and space filling carbonate found in veins, like that seen at Reppia. Petrographic evidence shows that this post-dates serpentinization and talc alteration, and is similar to what is found on the seafloor (e.g. Lost City & Ghost City; Fruh-Green et al., 2003).

Stable isotope data and carbon contents of our samples provide evidence that carbonates in these serpentinites were formed on the seafloor and preserved through obduction processes. Calcite and dolomites show no signs of secondary alteration processes and have isotopic signatures that are similar to carbonates forming at modern UM hosted hydrothermal systems (Figure 14). Carbonated serpentinites from Reppia all fall within the range of a multitude of seafloor sites (eg. Lost City, Ghost City, Iberian Margin; Fruh-Green et al., 2003; Lautuad et al., 2011; Schwarzenbach et al., 2013).

Bulk rock carbon contents and  $\delta^{13}\text{C}$  values are also consistent with a seafloor origin. Total carbon contents of seafloor serpentinites fall along a mixing line between small amounts of a low- $\delta^{13}\text{C}$  organic component and large amounts of seawater carbonate having  $\delta^{13}\text{C} \sim 1\%$  (Figure 16; Alt et al., 2013). The serpentinites analyzed in this study plot along the same mixing line. These high  $\delta^{13}\text{C}$  values are consistent with formation from seawater. There is a slight decrease in the  $\delta^{13}\text{C}$  values for the fault rocks, which may result from fluids containing reduced carbon species, such as methane or a mantle  $\text{CO}_2$  component being transported in hydrothermal fluids through the fault zone. This is found at low-temperature UM systems such as Lost City on the Mid-Atlantic Ridge (Fruh-Green et al., 2004; Kelley et al., 2005).

Temperatures calculated from oxygen isotope analysis of calcite range from 20–95 °C. Fault zone carbonates contain mostly dolomite with minor calcite with temperatures that range from 91–123°C. These temperatures match the ranges of carbonate precipitates measured in low-temperature UM hydrothermal systems on the seafloor (Fruh-Green et al., 2003). Carbonate precipitation in these systems occurs from the mixing of hydrothermal fluids (Ca-rich) with seawater ( $\text{CO}_2$ -rich) (Schwarzenbach et al., 2013). Two carbonate-rich serpentinite breccias have an REE signature similar to that of black smoker fluid (Figure 10.D) with a well-defined

positive Eu anomaly, although they are much more enriched in REE. These rocks must have interacted with black smoker like hydrothermal fluids whilst on the seafloor which is supported by similar REE patterns measured in seafloor carbonates located at UM hydrothermal fields (Eickmann et al., 2009; Schroeder et al., 2015). The low Mg contents of the calcite in these rocks (Figure 13), is similar to calcite formed in equilibrium with seawater which is expected to contain 4–22 mol% MgCO<sub>3</sub> (Carpenter and Lohmann, 1992). There is little to no Mg in UM hydrothermal fluids, which necessitates mixing of hydrothermal fluids with seawater or reactions with the Mg-rich serpentinites to account for Mg concentrations of calcites and REE patterns. (Fouquet et al., 2010).

The MgO/SiO<sub>2</sub> ratios of the carbonate-bearing rocks decrease with increasing amount of alteration (Figure 8). The veined serpentinites have ratios of 0.69–0.84, the serpentinite breccias 0.56–0.66 and the fault zone rocks 0.4 to 0.53 (Figure 8). The more reacted the rocks, the more carbonate alteration and the greater change in major element compositions. This correlates with proximity to the fault zone, which acted as a focused fluid pathway (see below).

Bulk rock trace element data demonstrate the chemical effects associated with carbonate formation (Figure 12). Sr is clearly being incorporated into the carbonates, as seen by the higher Sr concentrations associated with carbonate-rich samples. The amount of Sr in these carbonated samples is 22–152 times the concentration in the background serpentinites. The elevated Sr concentrations are additional evidence for low-temperature precipitation because Sr partitioning into carbonate phases increases greatly at low-temperatures (Kinsman, 1969).

### *Fault Rocks*

The massive sulfides situated at the top of the fault zone were formed by high-temperature, metal-bearing fluids that were focused into a fluid conduit controlled by the fault. Massive sulfides of the N. Apennines contain between 1.67–5.08 wt% copper (Zaccarini and Garuti, 2008). For such a large amount of metals to be transported in solution and eventually deposited, it has been shown experimentally that fluid temperatures need to be  $> 350^{\circ}\text{C}$  (Seewald and Seyfried, 1990). Further evidence of high-temperature fluids transported through this fault conduit are the chloritized basalts that flank both sides of the fault zone. These basalts have been completely replaced by chlorite, which has been shown by chlorite geothermometry (Kraniotis and MacLean, 1987) to require temperatures  $> 200^{\circ}\text{C}$  (Natland et al., 1982; Zaccarini and Garuti, 2008). There is also minor pyrite + chalcopyrite + sphalerite + pyrrhotite that occur with carbonates in the fault zone.

Fault zone carbonates consist of dolomites and minor calcite with formation temperatures that range from  $91\text{--}123^{\circ}\text{C}$ , depending on the fluid composition (seawater or hydrothermal fluids). The low temperatures for these carbonates is evidence that after the high-temperature alteration, cooler fluids took advantage of the same fluid conduits. When hot, UM hydrothermal fluids cool they become more alkaline and precipitate carbonates when mixed with seawater (Foustoukos, 2008). Carbonate temperatures decrease away from the fault zone, but increase again  $\sim 45$  m away from the fault zone where the mineralized + talc altered serpentinite occurs (Figure 17), suggesting another zone of focused fluid flow. Cu concentrations show a very similar pattern (Figure 18), with a maximum in the fault zone, a decrease away from the fault, and then elevated values in the mineralized talc altered serpentinites. These elevated temperatures and Cu enrichment may be linked to the main fault conduit and sulfide mineralization, but the connection is not clear due to lack of exposed rocks.

The carbonate-rich fault zone rocks could be replacement products of serpentine or precipitates from hydrothermal fluids. By comparing metal contents of the fault rocks to background serpentinites (Figure 9), this can be assessed. Metals such as Cu, Ni and Zn can be mobilized by hydrothermal fluids so the variable concentrations in the different rock types suggest a hydrothermal origin. The depletion of Cr in the talc altered rocks is caused by the destruction of the Cr-bearing phase (Cr-spinel) during silicification. Cr is present in the serpentinites and carbonate-veined serpentinite as Cr-spinel, which was also identified in carbonate-rich fault zone breccias. The presence of angular, broken detrital grains of Cr-spinel in the massive sulfide deposits of Reppia was noted by Garuti and Zaccarini, (2005). This contrasts with the globular primary morphology of spinel in the Reppia fault rocks (Figure 6.F), evidence that these grains are not detrital and preserved in the rock, suggesting a replacement origin for the carbonate-rich fault rocks.

The bulk rock composition of the carbonates-rich fault zone rocks is additional evidence for an origin by replacement of serpentinites. The low MgO/SiO<sub>2</sub> concentrations of the fault rocks show that these rocks lost Mg. Hydrothermal fluids contain zero Mg and it is likely that focused flow of these fluids through the rocks leached Mg. (Fouquet, 2010). It has also been shown that seawater in the Jurassic (when these rocks were exposed on the seafloor) was characterized by higher Ca/Mg ratios (Geloni and Gianelli, 2007). Mg was lost from the bulk rocks, but some Mg remained in the rocks through dolomite formation. Dolomite and quartz formation are expected at the end of reaction pathways of CO<sub>2</sub> rich seawater reacting with serpentinites at 100 °C, which is similar to what is observed at Reppia (Klein and Garrido, 2011). The dolomites are also Fe-rich, and fault rocks are elevated in FeO (>10 wt%) compared to background serpentinites (8.6 wt%). Additional Fe was most likely added by high temperature

fluids (~350°C), because black smoker fluids that vent in UM hydrothermal systems are elevated in metals and able to transport dissolved Fe much more readily than low temperature fluids (Seyfried et al., 2011). This Fe was then reacted with infiltrating fluids during fluid circulation to form these replacive Fe-dolomites. Compositions of altered rocks preserve evidence of a mixture of seawater and hydrothermal fluids mixing in the fault conduit to create the observed alteration.

REE patterns show evidence of extensive interaction with hydrothermal fluids (Figure 10). The REE patterns of these fault rocks are extremely elevated when compared to the background IL peridotite. LREE are the most elevated, having concentrations up to 23x greater than the IL peridotite composition. HREE concentrations are lower than the LREE concentrations, but are still 3x greater than the IL peridotite. Schroeder et al., (2015) and Eickmann et al., (2015) have shown that hydrothermal calcite and dolomite in seafloor serpentinites can preserve similar (or greater) elevated REE concentrations. These elevated REE signatures commonly preserve a positive Eu anomaly that records a hydrothermal fluid origin, but this is not always present due to the redox state of the fluids. The ionic radius of  $\text{Eu}^{2+}$  is too big to fit into Mg-Fe carbonates, while  $\text{Eu}^{3+}$  can easily fit into the  $\text{Mg}^{2+}$  or  $\text{Fe}^{2+}$  sites (Bau and Moller, 1992). Thus the REE in the fault zone dolomites record the effects of hydrothermal fluids, but Eu contents of the carbonates were controlled by redox during mixing of reduced hydrothermal fluids and oxidized seawater.

## **Conclusions**

After combining field site observations with detailed petrology and geochemistry, we propose that the ophiolites preserved in the Reppia area of the Internal Ligurides preserve rocks with a primary seafloor serpentization signature and evidence for two distinct stages of

seafloor UM hydrothermal systems. More precisely, they preserve the evidence of high temperature alteration ( $>350^{\circ}\text{C}$ ) that occurs from the expulsion of hot, metal-rich fluids that vent at black smokers and form massive sulfide deposits on the seafloor. Also preserved is the later effect of cooler fluids that occurs when thermal supply diminishes, and carbonate formation becomes the dominant alteration.

The field site in Reppia serves as a unique proxy to UM seafloor systems, because it preserves the subsurface beneath an oceanic detachment fault, exposing the high angle normal faults which acted as conduits for hydrothermal fluids to travel upward from deeper in the subsurface. The data clearly demonstrates the strong control that faults have on transporting fluids. It has been proposed that after exhumation of serpentinites to the seafloor, additional deformation is accommodated by a network of normal faults that cut the massif (Tucholke et al., 2008). These faults are vital for providing an extended network for fluid circulation of both active and fossil hydrothermal fields (Andreani et al., 2014). This interpretation fits well with observations and geochemical data from the field site, which is a well-preserved proxy of a seafloor, UM hydrothermal system.

We also conclude that the normal fault was able to focus fluids, and act as a “fault upflow zone” which encouraged a large amount of fluid/rock interactions with fluids of various temperatures. Understanding the mechanics of these faults and how they are able to focus fluids from depth, will help with better understanding detachment subsurface processes that lead to formation of VMS deposits or the seafloor carbon cycle which can potentially help with sequestering global  $\text{CO}_2$ .

## References

- Alt, J.C., Shanks III, W.C., 2003. Serpentinization of abyssal peridotites from the MARK area, Mid-Atlantic Ridge: sulfur geochemistry and reaction modeling. *Geochim. Cosmochim. Acta* 67, 641–653.
- Alt, J.C., Shanks, W.C., Bach, W., Paulick, H., Garrido, C.J., Beaudoin, G., 2007. Hydrothermal alteration and microbial sulfate reduction in peridotite and gabbro exposed by detachment faulting at the Mid-Atlantic Ridge, 15° 20'N (ODP Leg 209): A sulfur and oxygen isotope study. *Geochemistry, Geophys. Geosystems* 8.
- Alt, J.C., Shanks, W.C., Crispini, L., Gaggero, L., Schwarzenbach, E.M., Früh-Green, G.L., Bernasconi, S.M., 2012. Uptake of carbon and sulfur during seafloor serpentinization and the effects of subduction metamorphism in Ligurian peridotites. *Chem. Geol.* 322-323, 268–277.
- Alt, J.C., Schwarzenbach, E.M., Früh-Green, G.L., Shanks, W.C., Bernasconi, S.M., Garrido, C.J., Crispini, L., Gaggero, L., Padrón-Navarta, J. A., Marchesi, C., 2013. The role of serpentinites in cycling of carbon and sulfur: Seafloor serpentinization and subduction metamorphism. *Lithos* 178, 40–54.
- Andersen, C., Rupke, L., Hasenclever, J., Grevemeyer, I., Petersen, S., 2015. Fault geometry and permeability contrast control vent temperatures at the Logatchev 1 hydrothermal field, Mid-Atlantic Ridge. *Geology* 43, 51–54.
- Andreani, M., Mével, C., Boullier, A. M., Escartín, J., 2007. Dynamic control on serpentine crystallization in veins: Constraints on hydration processes in oceanic peridotites. *Geochemistry, Geophys. Geosystems* 8.
- Andreani, M., Escartin, J., Ildefonse, B., Godard, M., 2014. Tectonic structure, lithology, and hydrothermal signature of the Rainbow massif (Mid-Atlantic Ridge 36°14'N) 1–29.
- Bach, W., Garrido, C.J., Paulick, H., Harvey, J., Rosner, M., 2004. Seawater-peridotite interactions: First insights from ODP Leg 209, MAR 15°N. *Geochemistry, Geophys. Geosystems* 5.
- Bach, W., Rosner, M., Jöns, N., Rausch, S., Robinson, L.F., Paulick, H., Erzinger, J., 2011. Carbonate veins trace seawater circulation during exhumation and uplift of mantle rock: Results from ODP Leg 209. *Earth Planet. Sci. Lett.* 311, 242–252.
- Barrett, T.J., Friedrichsen, H., 1989. Stable isotopic composition of atypical ophiolitic rocks from east Liguria, Italy. *Chem. Geol. Isot. Geosci. Sect.* 80, 71–84.
- Bau, M., Moller, P., 1992. Rare earth element fractionation in metamorphogenic hydrothermal calcite, magnesite and siderite. *Mineral. Petrol.* 45, 231–246.



- Beard, J.S., Frost, B.R., Fryer, P., McCaig, A., Searle, R., Ildefonse, B., Zinin, P., Sharma, S.K., 2009. Onset and progression of serpentinization and magnetite formation in Olivine-rich troctolite from IODP hole U1309D. *J. Petrol.* 50, 387–403.
- Blackman, D.K., Canales, J.P., Harding, A., 2009. Geophysical signatures of oceanic core complexes. *Geophys. J. Int.* 178, 593–613.
- Bodinier, J.L., Godard, M., 2013. Orogenic, Ophiolitic, and Abyssal Peridotites. *Treatise Geochemistry Second Ed.* 3, 103–167.
- Cannat, M., Fontaine, F., Escartín, J., 2010. Serpentinization and Associated Hydrogen and Methane Fluxes at Slow Spreading Ridges. *Divers. Hydrothermal Syst. Slow Spreading Ocean Ridges* 241–264.
- Carpenter, S.J., Lohmann, K.C., 1992. Sr Mg ratios of modern marine calcite: Empirical indicators of ocean chemistry and precipitation rate. *Geochim. Cosmochim. Acta* 56, 1837–1849.
- Dick, H.J.B., Fisher, R.L., Bryan, W.B., 1984. Mineralogic variability of the uppermost mantle along mid-ocean ridges. *Earth Planet. Sci. Lett.* 69, 88–106.
- Douville, E., Charlou, J.L., Oelkers, E.H., Bienvenu, P., Jove Colon, C.F., Donval, J.P., Fouquet, Y., Prieur, D., Appriou, P., 2002. The rainbow vent fluids (36°14'N, MAR): The influence of ultramafic rocks and phase separation on trace metal content in Mid-Atlantic Ridge hydrothermal fluids. *Chem. Geol.* 184, 37–48.
- Eickmann, B., Bach, W., Rosner, M., Peckmann, J., 2009. Geochemical constraints on the modes of carbonate precipitation in peridotites from the Logatchev Hydrothermal Vent Field and Gakkel Ridge. *Chem. Geol.* 268, 97–106.
- Escartín, J., and J. P. Canales (2011), Detachments in oceanic lithosphere: Deformation, magmatism, fluid flow, and ecosystems, *Eos Trans. AGU*, 92(4).
- Fouquet, Y., Cambon, P., Etoubleau, J., Charlou, J.L., Ondreas, H., Barriga, F.J.A.S., Cherkashov, G., Semkova, T., Poroshina, I., Bohn, M., Donval, J.P., Henry, K., Murphy, P., and Rouxel, O., 2010. Geodiversity of Hydrothermal Processes Along the Mid-Atlantic Ridge and Ultramafic-Hosted Mineralization: a New Type Of Oceanic Cu-Zn-Co-Au Volcanogenic Massive Sulfide Deposit, In: *Diversity of Hydrothermal Systems on Slow Spreading Ocean Ridges* 188, 321–367.
- Foustoukos, D.I., Savov, I.P., Janecky, D.R., 2008. Chemical and isotopic constraints on water/rock interactions at the Lost City hydrothermal field, 30°N Mid-Atlantic Ridge. *Geochim. Cosmochim. Acta* 72, 5457–5474.

- Friedman, I., O'Neil, J.R., 1977. Data of Data of Geochemistry Sixth Edition. Geol. Surv. Prof. Pap. 440-KK, 1–117.
- Frost, B.R., Evans, K.A., Swapp, S.M., Beard, J.S., Mothersole, F.E., 2013. The process of serpentinization in dunite from New Caledonia. *Lithos* 178, 24–39.
- Früh-green, A.G.L., Kelley, D.S., Bernasconi, S.M., Jeffrey, A., Ludwig, K.A., Butterfield, D.A., Boschi, C., Proskurowski, G., 2003. 30,000 Years of Hydrothermal Activity at the Lost City. *Science*, 301, 495–498.
- Garuti, G., Zaccarini, F., 2005. Minerals of Au, Ag and U in volcanic-rock-associated massive sulfide deposits of the northern apennine ophiolite, Italy. *Can. Mineral.* 43, 935–950.
- Garuti, G., Bartoli, O., Scacchetti, M., Zaccarini, F., 2008. Geological setting and structural styles of Volcanic Massive Sulfide deposits in the northern Apennines (Italy): evidence for sea floor and sub-seafloor hydrothermal activity in unconventional ophiolites of the Mesozoic Tethys. *Boletìn la Soc. Geològica Mex.* 60, 121–145.
- Garuti, G., Alfonso, P., Proenza, J.A., Zaccarini, F., 2009. Sulfur-isotope variations in sulfide minerals from massive sulfide deposits of the Northern Apennine ophiolites: Inorganic and biogenic constraints. *Ofioliti* 34, 43–62.
- Geloni, C., Gianelli, G., 2007. A preliminary geochemical model of the fluid-rock interaction processes forming the eastern Liguria ophiolite (northern Apennines, Italy). *Period. di Mineral.* 76, 137–154.
- German, C.R., Lin, J., 2004. The thermal structure of the oceanic crust, ridge-spreading and hydrothermal circulation: How well do we understand their inter-connections? *Mid-Ocean Ridges Hydrothermal Interact. Between Lithosph. Ocean.* 148, 1–18.
- Hart, S.R., Zindler, A., 1986. In search of a bulk-Earth composition. *Chem. Geol.* 57, 247–267.
- Hébert, R., Adamson, A. C., Komor, S.C., 1990. Metamorphic petrology of ODP Leg 109, Hole 670A serpentinized peridotites: serpentinization processes at a slow spreading ridge environment. *Proc. Ocean Drill. Program, Sci. Results* 106/109, 103–115.
- Jagoutz, E., Palme, H., Baddenhausen, H., Blum, K., Cendales, M., Dreibus, G., Spettel, B., Lorenz, V., Vanke, H., 1979. The abundance of major, minor and trace elements in the earth's mantle as derived from primitive ultramafic nodules. *Geochim. Cosmochim. Acta* 11, 2031–2050.
- Kelemen, P.B., Matter, J., Streit, E.E., Rudge, J.F., Curry, W.B., Blusztajn, J., 2011. Rates and Mechanisms of mineral carbonation in peridotite" in sit CO<sub>2</sub> capture and storage. *Annu. Rev. Earth Planet. Sci.* 39, 545–576.

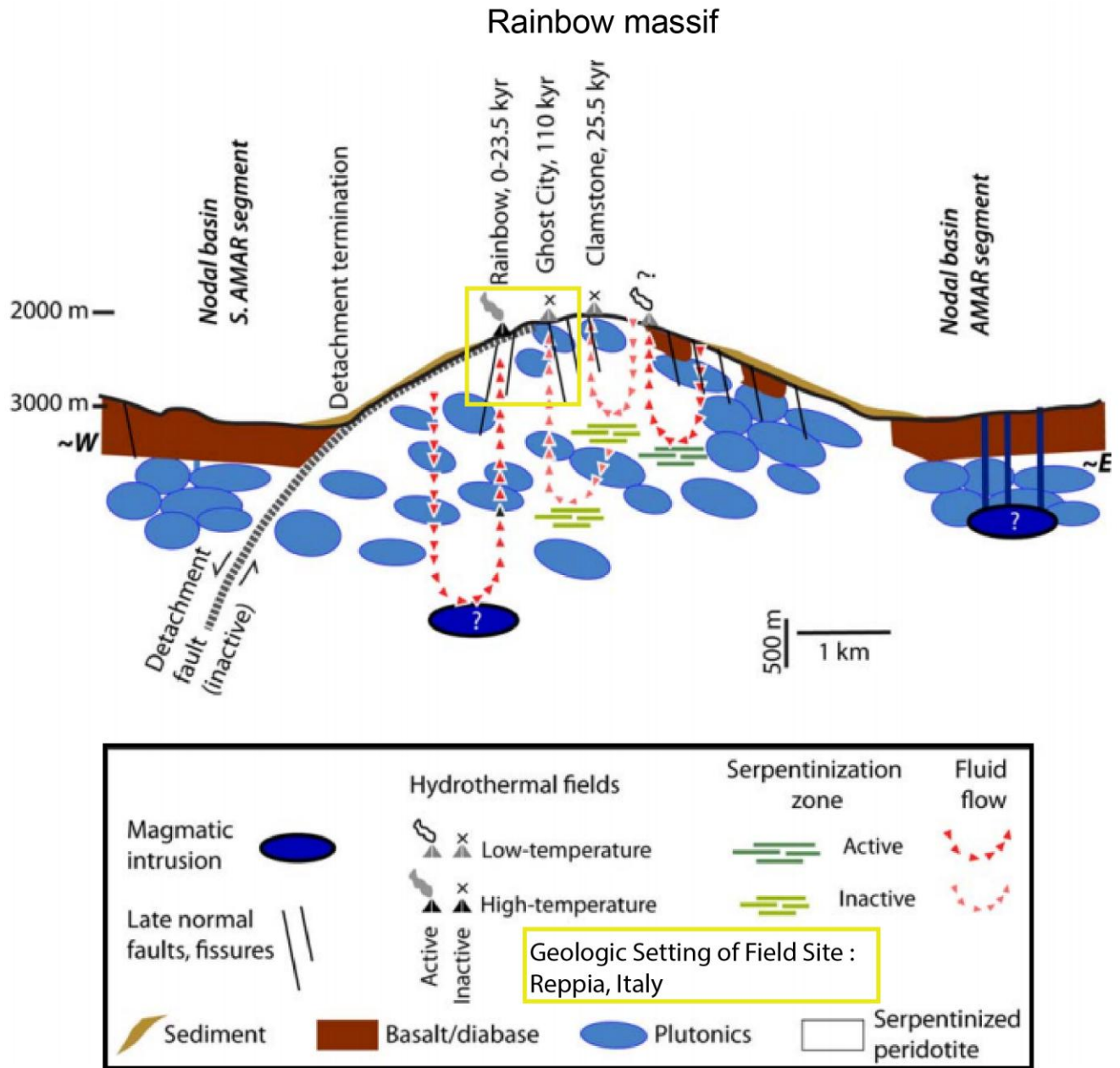
- Kelley, D.S., Karson, J.A., Blackman, D.K., Fruh-Green, G.L., Butterfield, D.A., Lilley, M.D., Olson, E.J., Schrenk, M.O., Roe, K.K., Lebon, G.T., Rivizzigno, P., 2001. An off-axis hydrothermal vent field near the Mid-Atlantic Ridge at 30 degrees N. *Nature* 412, 145–149.
- Kinsman, D.J.J., 1969. Interpretation of  $\text{Sr}^{2+}$  concentration in carbonate minerals and rocks. *J. Sediment. Petrol.* 39, 486–508.
- Klein, F., Garrido, C.J., 2011. Thermodynamic constraints on mineral carbonation of serpentinized peridotite. *Lithos* 126, 147–160.
- Kranidiotis P, MacLean WH., 1987. Systematics of chlorite alteration at the Phelps Dodge massive sulfide deposit, Matamagi, Quebec. *Econ Geol* 82:1898–1911
- Lartaud, F., Little, C.T.S., de Rafelis, M., Bayon, G., Dymont, J., Ildefonse, B., Gressier, V., Fouquet, Y., Gaill, F., Le Bris, N., 2011. Fossil evidence for serpentinization fluids fueling chemosynthetic assemblages. *Proc. Natl. Acad. Sci. U. S. A.* 108, 7698–7703.
- Lemoine, M., Tricart, P., Boillot, G., 1987. Ultramafic and gabbroic ocean floor of the Ligurian Tethys (Alps, Corsica, Apennines): in search of a genetic model. *Geology* 15, 622–625. 2
- Lowell, R.P., 2010. Hydrothermal systems at slow-spreading ridges: Analysis of heat sources and heat transfer processes. *Divers. Hydrothermal Syst. Slow Spreading Ridges* 188, 11–26.
- Malvoisin, B., 2015. Mass transfer in the oceanic lithosphere: Serpentinization is not isochemical. *Earth Planet. Sci. Lett.* 430, 75–85.
- McCaig, A.M., Delacour, A., Fallick, A.E., Castelain, T., Früh-Green, G.L., 2010. Detachment Fault Control on Hydrothermal Circulation Systems: Interpreting the Subsurface Beneath the TAG Hydrothermal Field Using the Isotopic and Geological Evolution of Oceanic Core Complexes in the Atlantic. *Divers. Hydrothermal Syst. Slow Spreading Ocean Ridges* 207–239.
- McDonough, W.F., Sun, S. -S., 1995. The Composition of the Earth. *Chem. Geol.* 120, 223-25.
- Muntener, O., Piccardo, G.B., 2003. Melt migration in ophiolitic peridotites: the message from Alpine-Apennine peridotites and implications for embryonic ocean basins. *Geol. Soc. London, Spec. Publ.* 218, 69–89.
- Natland, J.H., Hekinian, R., 1982. Hydrothermal Alteration of Basalts and Sediments at Deep Sea Drilling Project Site 456, Mariana Trough. *Deep. Drill. Proj. Initial Reports* 60, 759–767.
- Niu, Y., 2004. Bulk-rock major and trace element compositions of abyssal peridotites: Implications for mantle melting, melt extraction and post-melting processes beneath Mid-Ocean ridges. *J. Petrol.* 45, 2423–2458.

- Paulick, H., Bach, W., Godard, M., De Hoog, J.C.M., Suhr, G., Harvey, J., 2006. Geochemistry of abyssal peridotites (Mid-Atlantic Ridge, 15°20'N, ODP Leg 209): Implications for fluid/rock interaction in slow spreading environments. *Chem. Geol.* 234, 179–210.
- Pertsev, A. N., Bortnikov, N.S., Vlasov, E. a., Beltenev, V.E., Dobretsova, I.G., Ageeva, O. A., 2012. Recent massive sulfide deposits of the Semenov ore district, Mid-Atlantic Ridge, 13°31' N: Associated rocks of the oceanic core complex and their hydrothermal alteration. *Geol. Ore Depos.* 54, 334–346.
- Peters, M., Strauss, H., Farquhar, J., Ockert, C., Eickmann, B., Jost, C.L., 2010. Sulfur cycling at the Mid-Atlantic Ridge: A multiple sulfur isotope approach. *Chem. Geol.* 269, 180–196.
- Petersen, S., Herzig, P.M., Hannington, M.D., 2000. Third dimension of a presently forming VMS deposit: TAG hydrothermal mound, Mid-Atlantic Ridge, 26°N. *Miner. Depos.* 35, 233–259.
- Piccardo, G.B., Rampone, E., Romairone, A., 2002. Formation and composition of the oceanic lithosphere of the Ligurian Tethys: Inferences from the Ligurian ophiolites. *Ofioliti* 27, 145–162.
- Piccardo, G.B., 2008. The Jurassic Ligurian Tethys, a fossil ultraslow-spreading ocean; the mantle perspective. *Metasomatism in Ocean. Cont. lithospheric mantle* 11–34.
- Rampone, E., Hofmann, A. W., Piccardo, G.B., Vannucci, R., Bottazzi, P., Ottolini, L., 1996. Trace element and isotope geochemistry of depleted peridotites from an N-MORB type ophiolite (Internal Liguride, N. Italy). *Contrib. to Mineral. Petrol.* 123, 61–76.
- Ribeiro Da Costa, I., Barriga, F.J.A.S., Taylor, R.N., 2008. Late seafloor carbonate precipitation in serpentinites from the Rainbow and Saldanha sites (Mid-Atlantic Ridge). *Eur. J. Miner.* 20, 173–181.
- Rice, C.A., Tuttle, M.L., Reynolds, R.L., 1993. The analysis of forms of sulfur in ancient sediments and sedimentary rocks: comments and cautions. *Chem. Geol.* 107, 83–95.
- Rösli, U., Hoernes, S., Köppel, V., 1991. Isotope data of metarodingites and associated rocks from the Lanzo and Bracco ophiolitic massif: indication on the evolution of the Alpino-type ultramafic-mafic complexes. *Schweizerische Mineral. und Petrogr. Mitteilungen* 71, 125–141.
- Rouméjon, S., Cannat, M., 2014. Serpentinization of mantle derived peridotites at mid ocean ridges: mesh texture in the context of tectonic exhumation 2354–2379.
- Rouxel, O., Fouquet, Y., Ludden, J.N., 2004. Subsurface processes at the lucky strike hydrothermal field, Mid-Atlantic ridge: Evidence from sulfur, selenium, and iron isotopes. *Geochim. Cosmochim. Acta* 68, 2295–2311.

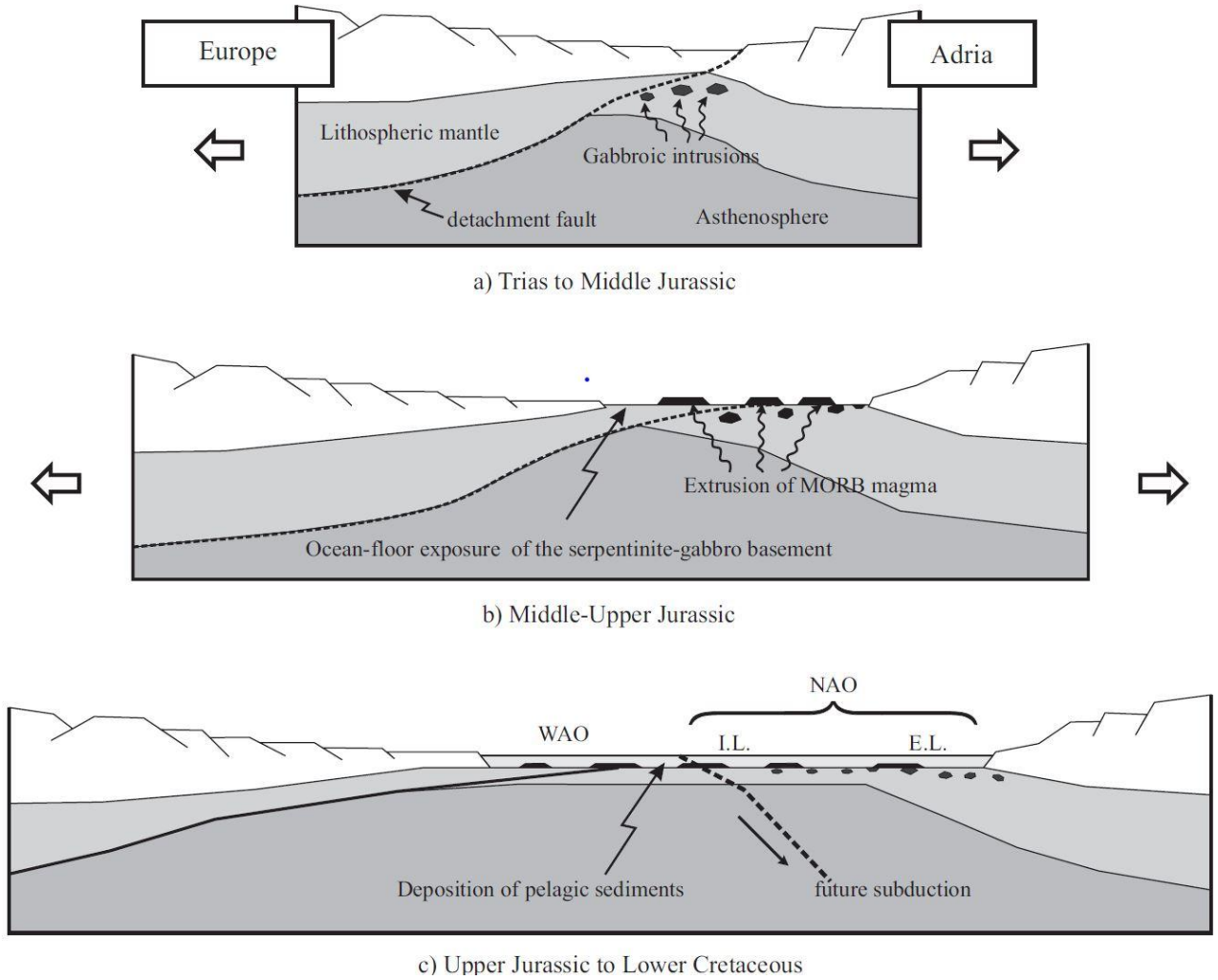
- Scambelluri, M., Piccardo, G. B., Philippot, P., Robbiano, A. & Negretti, L., 1997. High salinity fluid inclusions formed from recycled seawater in deeply subducted alpine serpentinite. *Earth and Planetary Science Letters*. 148, 485-500.
- Schmidt, K., Koschinsky, A., Garbe-Schönberg, D., de Carvalho, L.M., Seifert, R., 2007. Geochemistry of hydrothermal fluids from the ultramafic-hosted Logatchev hydrothermal field, 15°N on the Mid-Atlantic Ridge: Temporal and spatial investigation. *Chem. Geol.* 242, 1–21.
- Schrenk, M.O., Brazelton, W.J., Carolina, N., Lang, S.Q., 2013. Serpentinization, Carbon, and Deep Life. *Rev. Mineral.* 75, 575–606.
- Schroeder, T., W. Bach, N. Jons, S. Jons, P. Monien, and A. Klugel (2015), Fluid circulation and carbonate vein precipitation in the footwall of an oceanic core complex, Ocean Drilling Program Site 175, Mid-Atlantic Ridge, *Geochem. Geophys. Geosyst.*, 16, 3716– 3732,
- Schwarzenbach, E.M., Früh-Green, G.L., Bernasconi, S.M., Alt, J.C., Plas, A., 2013. Serpentinization and carbon sequestration: A study of two ancient peridotite-hosted hydrothermal systems. *Chem. Geol.* 351, 115–133.
- Seewald, J.S., Seyfried, W.E., 1990. The effect of temperature on metal mobility in subseafloor hydrothermal systems: constraints from basalt alteration experiments. *Earth Planet. Sci. Lett.* 101, 388–403.
- Seyfried, W.E., Pester, N.J., Ding, K., Rough, M., 2011. Vent fluid chemistry of the Rainbow hydrothermal system (36 °N, MAR): Phase equilibria and in situ pH controls on subseafloor alteration processes. *Geochim. Cosmochim. Acta* 75, 1574–1593.
- Smith, D. K., et al. (2014), Development and evolution of detachment faulting along 50 km of the Mid-Atlantic Ridge near 16.5°N, *Geochem. Geophys. Geosyst.*, 15, 4692–4711.
- Snow, J.E., Dick, H.J.B., 1995. Pervasive magnesium loss by marine weathering of peridotite. *Geochim. Cosmochim. Acta* 59, 4219–4235.
- Taylor, H.P., 1977. Water/rock interactions and the origin of H<sub>2</sub>O in granitic batholiths: Thirtieth William Smith lecture. *J. Geol. Soc. London*. 133, 509–558.
- Tucholke, B.E., Behn, M.D., Buck, W.R., Lin, J., 2008. Role of melt supply in oceanic detachment faulting and formation of megamullions. *Geology* 36, 455–458.
- Vasconcelos, C., McKenzie, J.A., Warthmann, R., Bernasconi, S.M., 2005. Calibration of the  $\delta^{18}\text{O}$  paleothermometer for dolomite precipitated in microbial cultures and natural environments. *Geology* 33, 317–320.

Zaccarini, F., Garuti, G., 2008. Mineralogy and chemical composition of VMS deposits of northern Apennine ophiolites, Italy: Evidence for the influence of country rock type on ore composition. *Mineral. Petrol.* 94, 61–83.

**Figures**

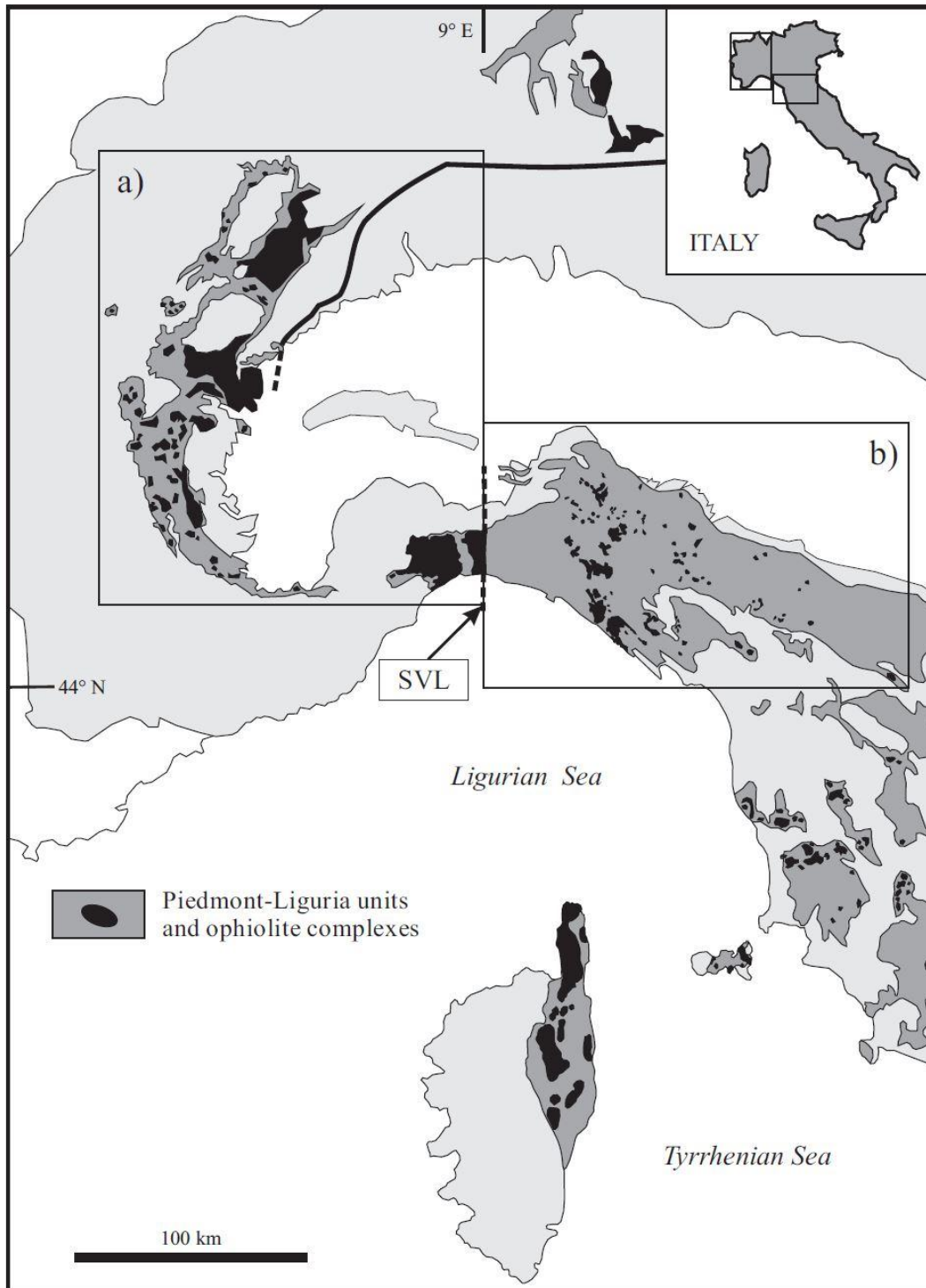


**Figure 1.** Geologic map showing the detachment surface of an oceanic core complex with hypothesized multiple faults cutting near active and inactive hydrothermal field on the seafloor. Inferred hydrothermal pathways and sources of heat are also shown. The yellow box depicts the setting of our field site that originated on the ocean floor (adapted from Andreani et al., 2014).

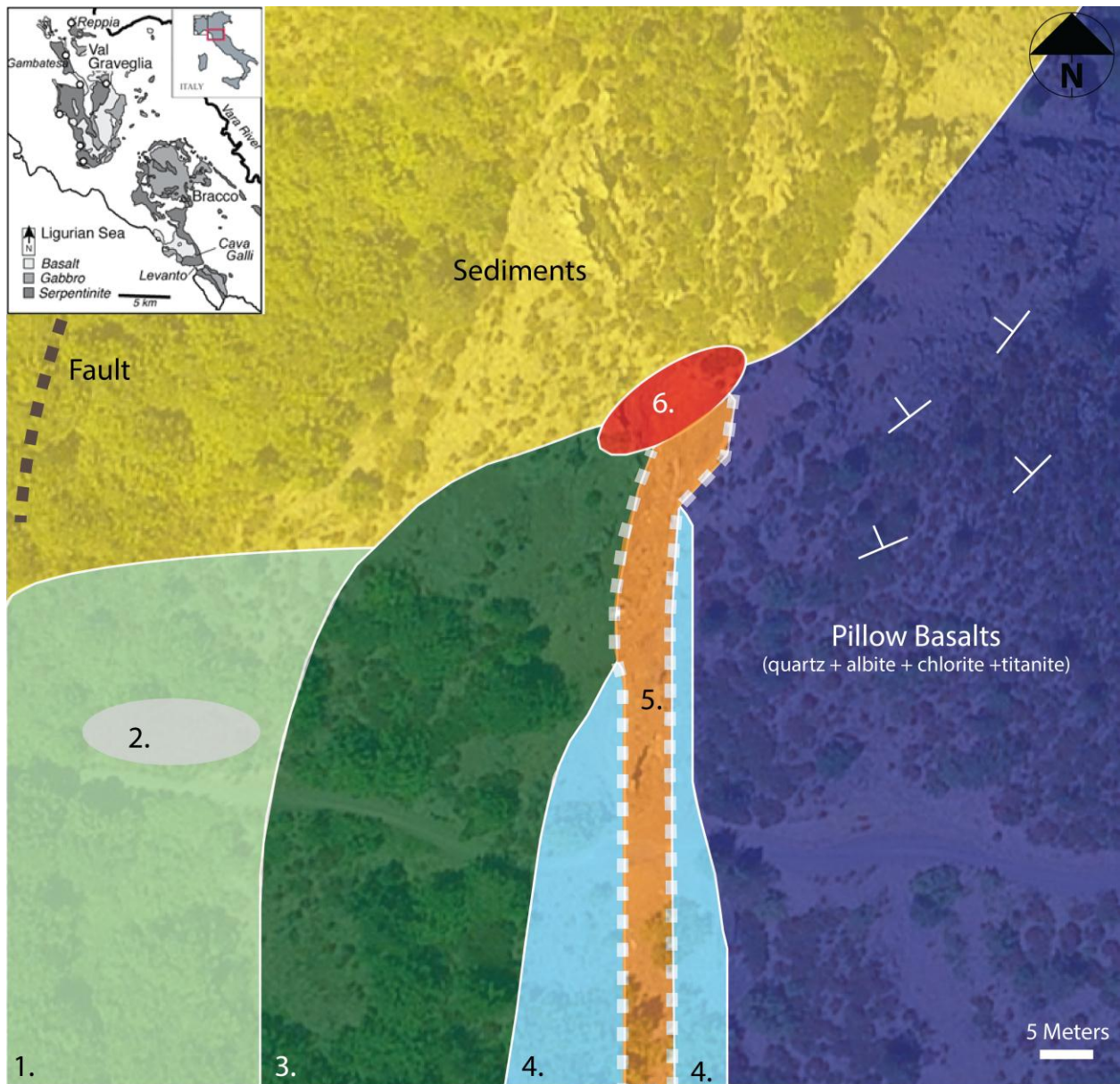


**Figure 2.** Schematic drawing showing the detachment fault that originated from the break-up of the Adria Plate from the European Plate resulting in the exhumation of sub-continental lithosphere that was then serpentinitized (from Garuti et al., 2008).





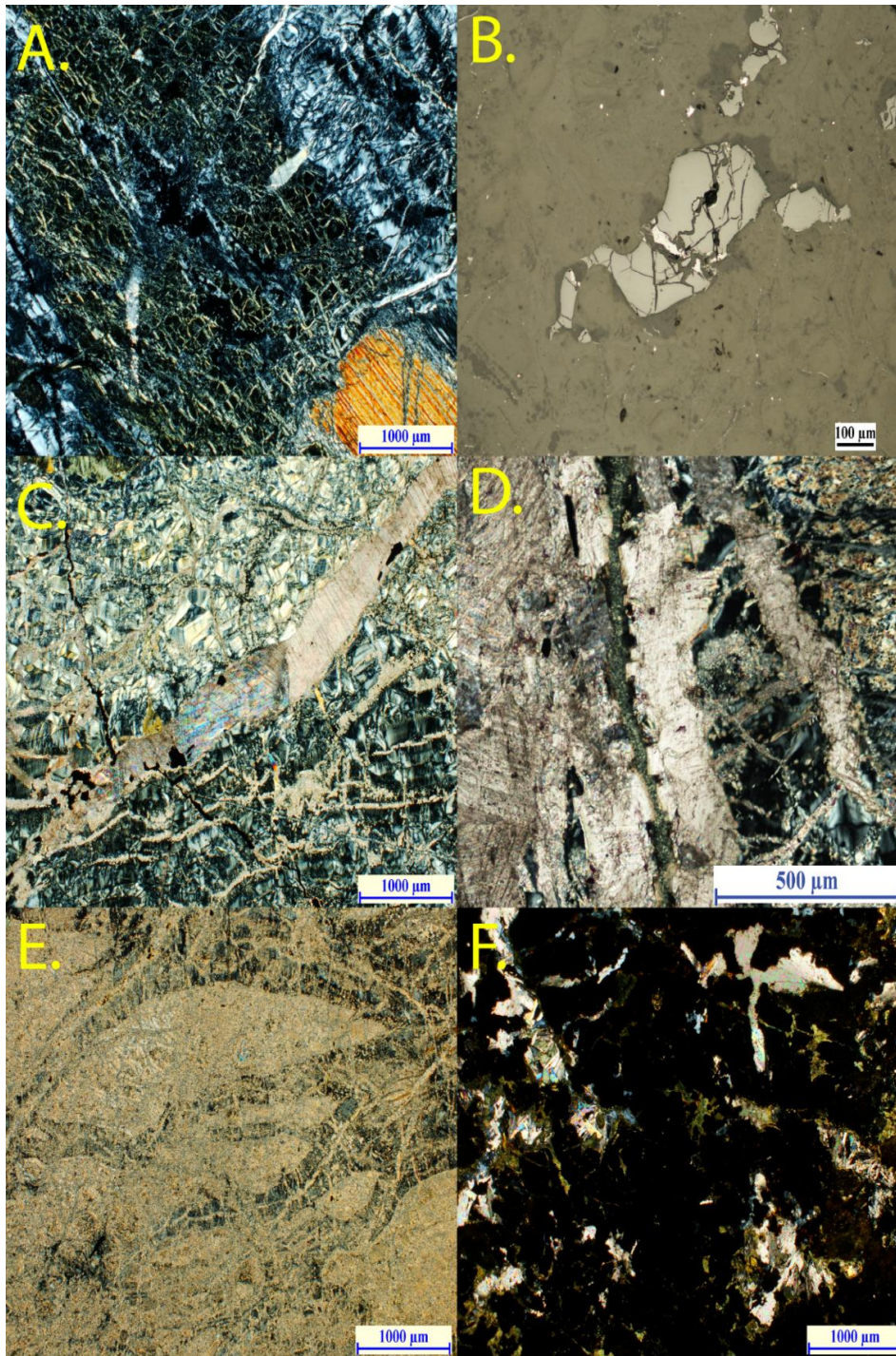
**Figure 3.** A map showing the structure and location of the Piedmont – Liguria units and ophiolite complexes. The rocks of the Northern Apennines preserve Prehnite-Pumpellyite facies to the east while rocks of the West Alps preserve eclogite- and blueschist facies-rocks to the west. They are separated by the Sestri-Vtaggio tectonic line (SVL) (from Garuti et al., 2008).



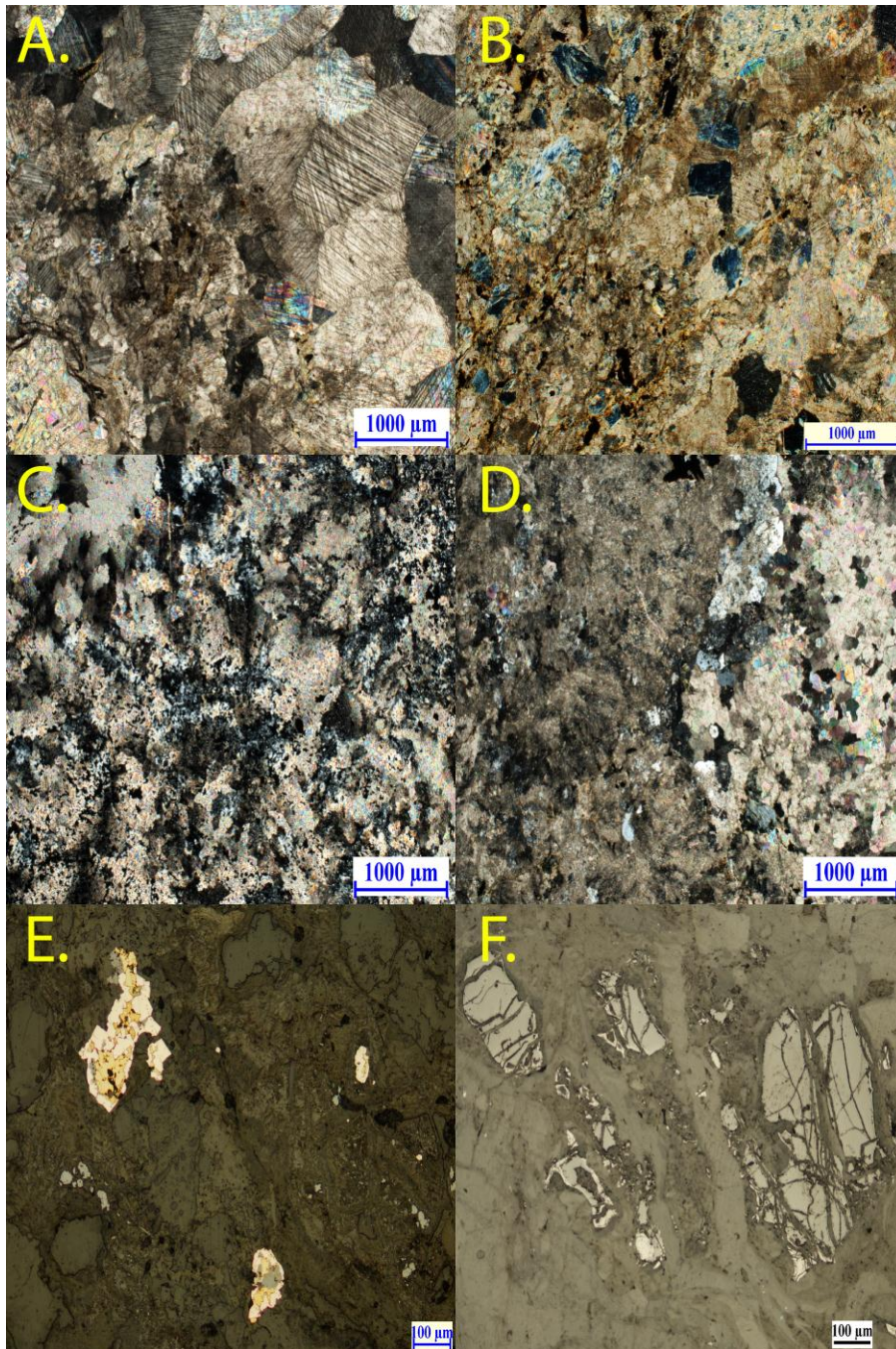
**Legend**

- 1. Carbonate Veined-Serpentinite
- 2. Mineralized Talc Altered Serpentinite
- 3. Serpentinite Breccia
- 4. Chloritized Basalt
- 5. Fault Zone Breccia
- 6. Massive Sulfide Deposit

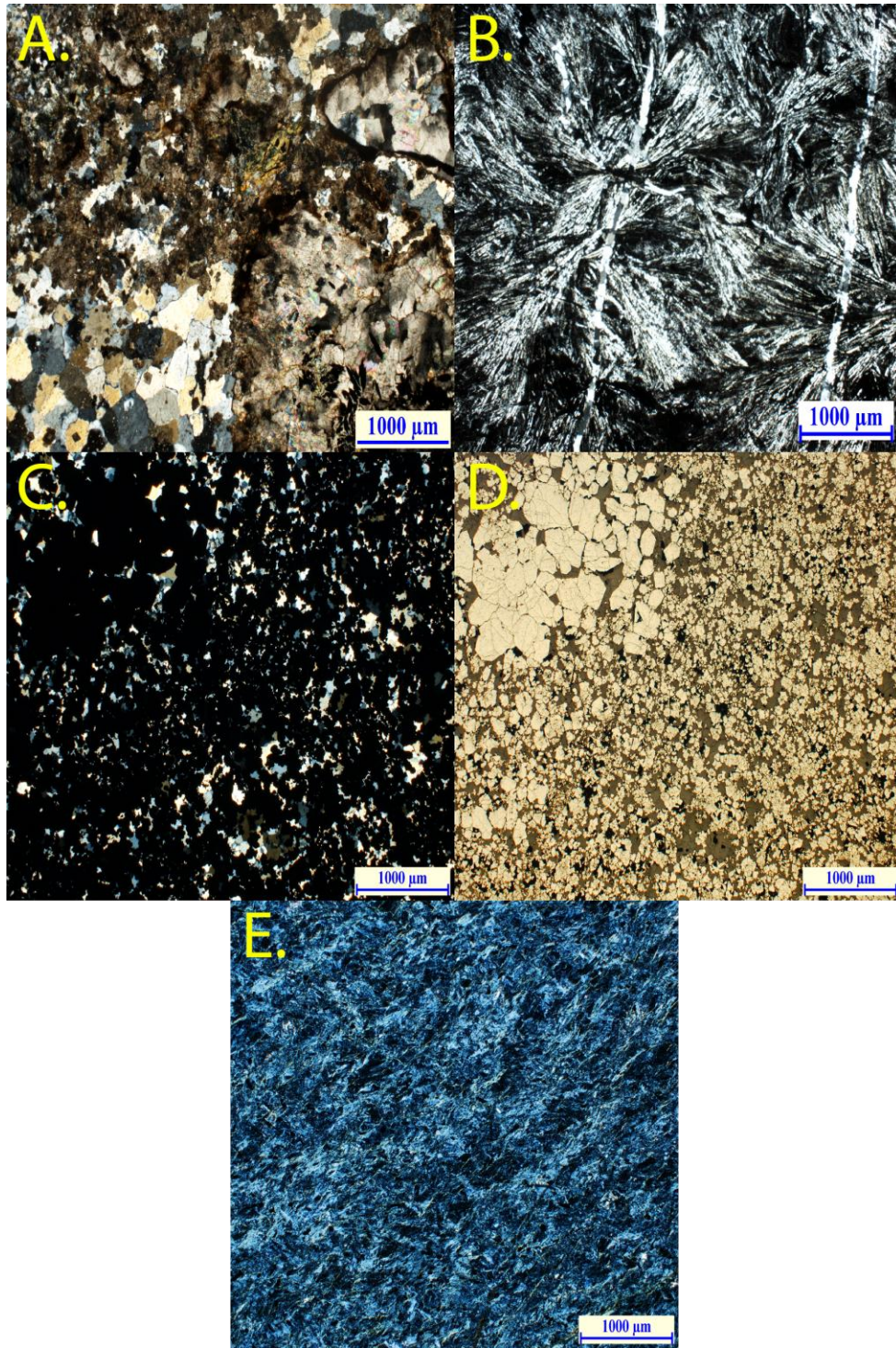
**Figure 4.** Geologic map of field site: Reppia, Italy (insert taken from Garuti et al., 2008).



**Figure 5.** Photomicrographs of thin sections showing mineralogy of different samples **A.** Background Serpentinite, showing serpentine and relict pyroxene. **B.** Background Serpentinite Cr-Spinel, showing rounded, globular, resorbed shape. **C.** Carbonate-Veined Serpentinite, showing calcite veins and smaller talc veins. **D.** Carbonate-Veined Serpentinite, showing calcite vein with “jagged” edges that replace wallrock serpentinite. **E.** Talc Altered Serpentinite, with relict serpentinite (dark) at upper right intensely veined and replaced by talc. **F.** Sulfide minerals (opaque) associated with Talc Altered Serpentinite.

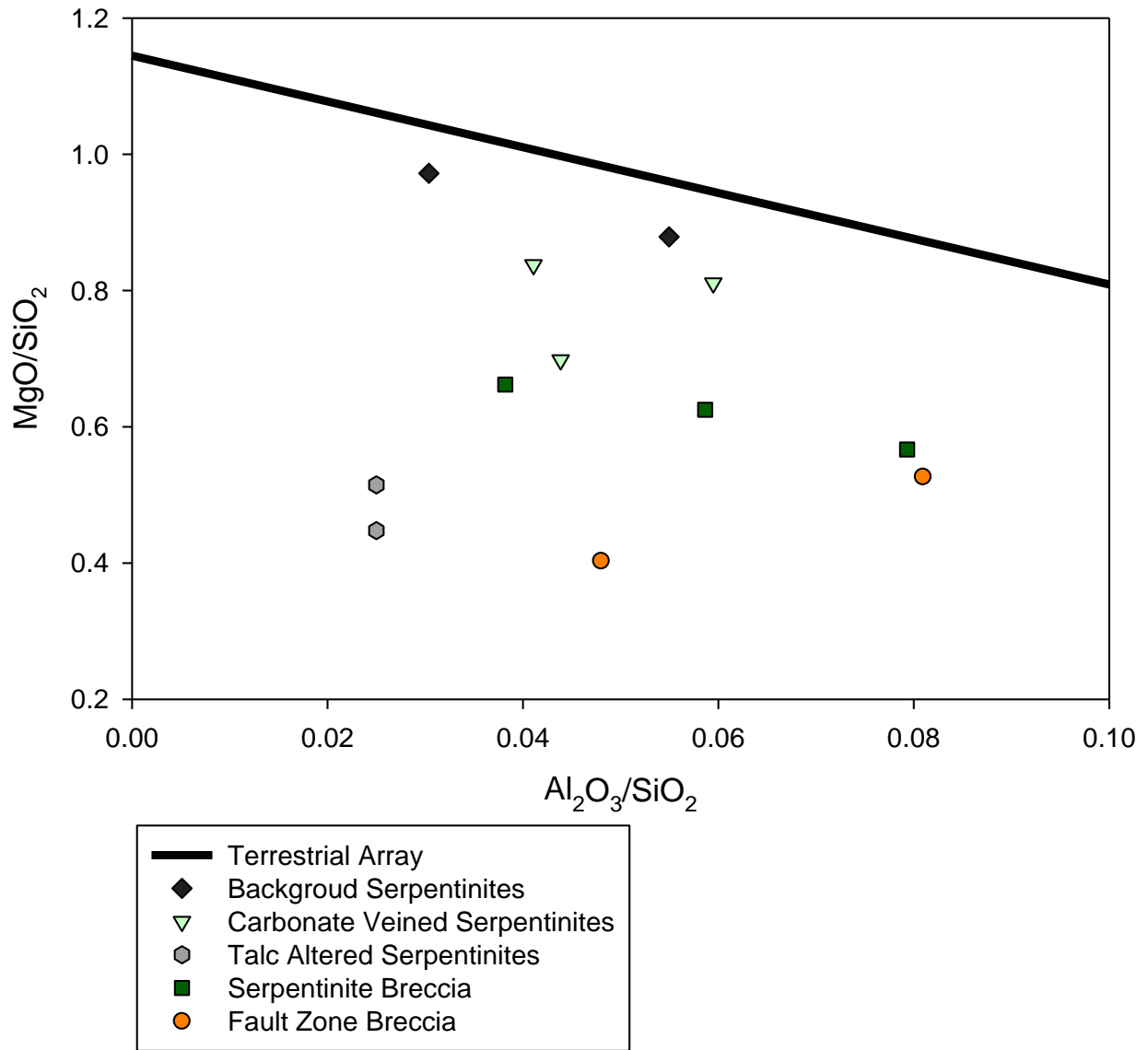


**Figure 6.** Photomicrographs of thin sections showing mineralogy of different samples found at field site. **A.** Serpentinite Breccia, showing sparry calcite cement composing the matrix. **B.** Serpentinite Breccia, showing sparry calcite and fine grained calcite cements with serpentine clasts partly replaced to talc and calcite. **C.** Fault-Zone Breccia, showing light and dark feathery carbonates that are composed of Fe-rich dolomite with minor calcite. **D.** Fault-Zone Breccia, showing feathery and euhedral rhomb carbonates **E.** Pyrite, chalcopyrite and sphalerite (gray, at bottom) associated w/ Fault-Zone Breccia that is replacing background serpentinite (reflected light). **F.** Fault Zone Breccia Cr-spinel is highly altered and fragmented/brecciated, but retains overall globular shape like in background serpentinite (reflected light).



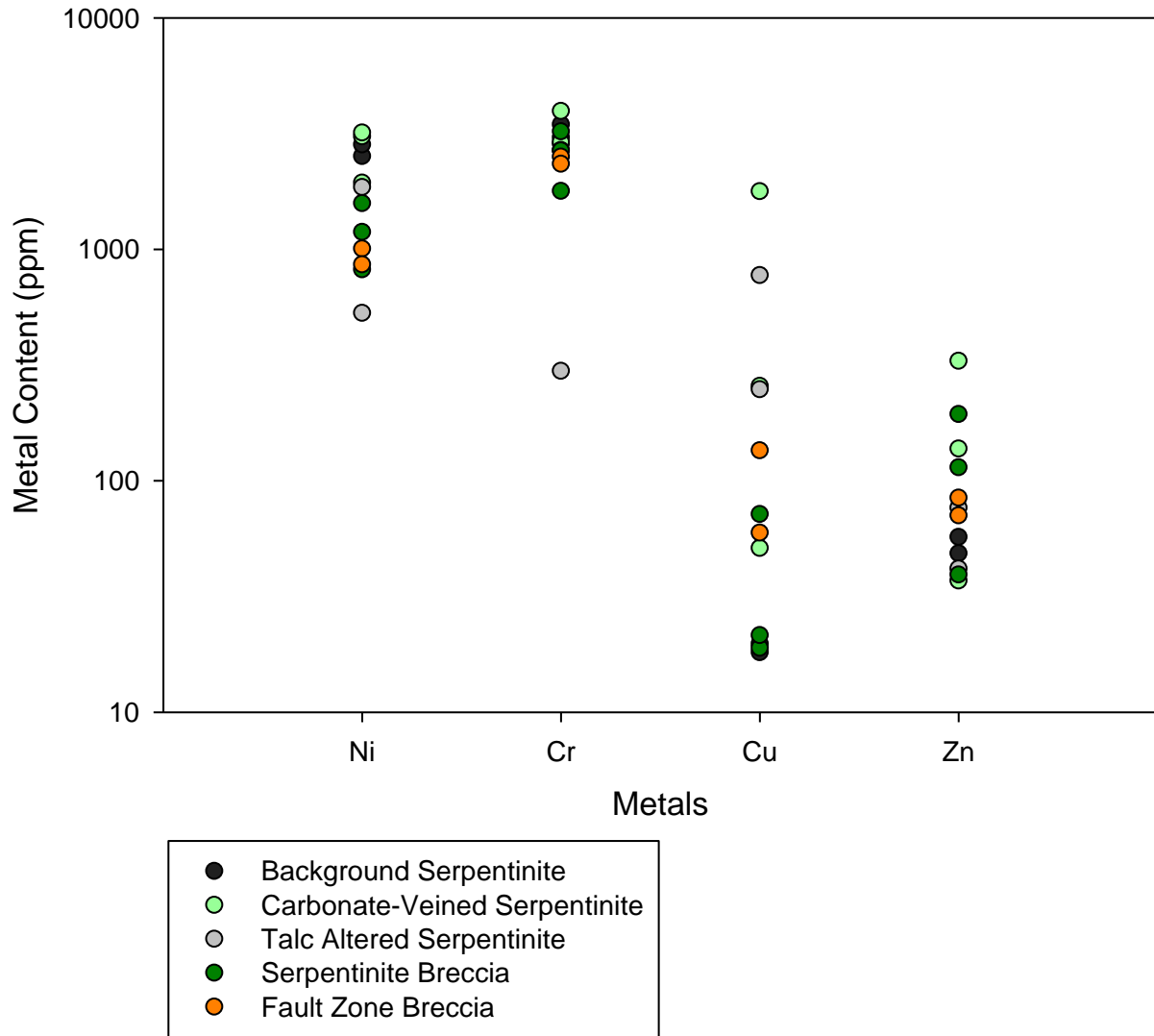
**Figure 7.** Photomicrographs of thin sections showing mineralogy of different samples found at field site. **A.** Fault Zone Breccia (70184-2), composed of carbonates, quartz and laths of hematite with Fe-oxyhydroxides. **B.** Hanging Wall Basalt, composed of albite, quartz with minor chlorite + titanite and showing relict basalt texture. **C.** Massive Sulfide Host Basalts (XPL), showing sulfides (opaque) and quartz. **D.** Massive Sulfide Host Basalts (combined reflected and transmitted light), showing pyrite. **E.** Chloritized Basalt

## Major Element Comparisons

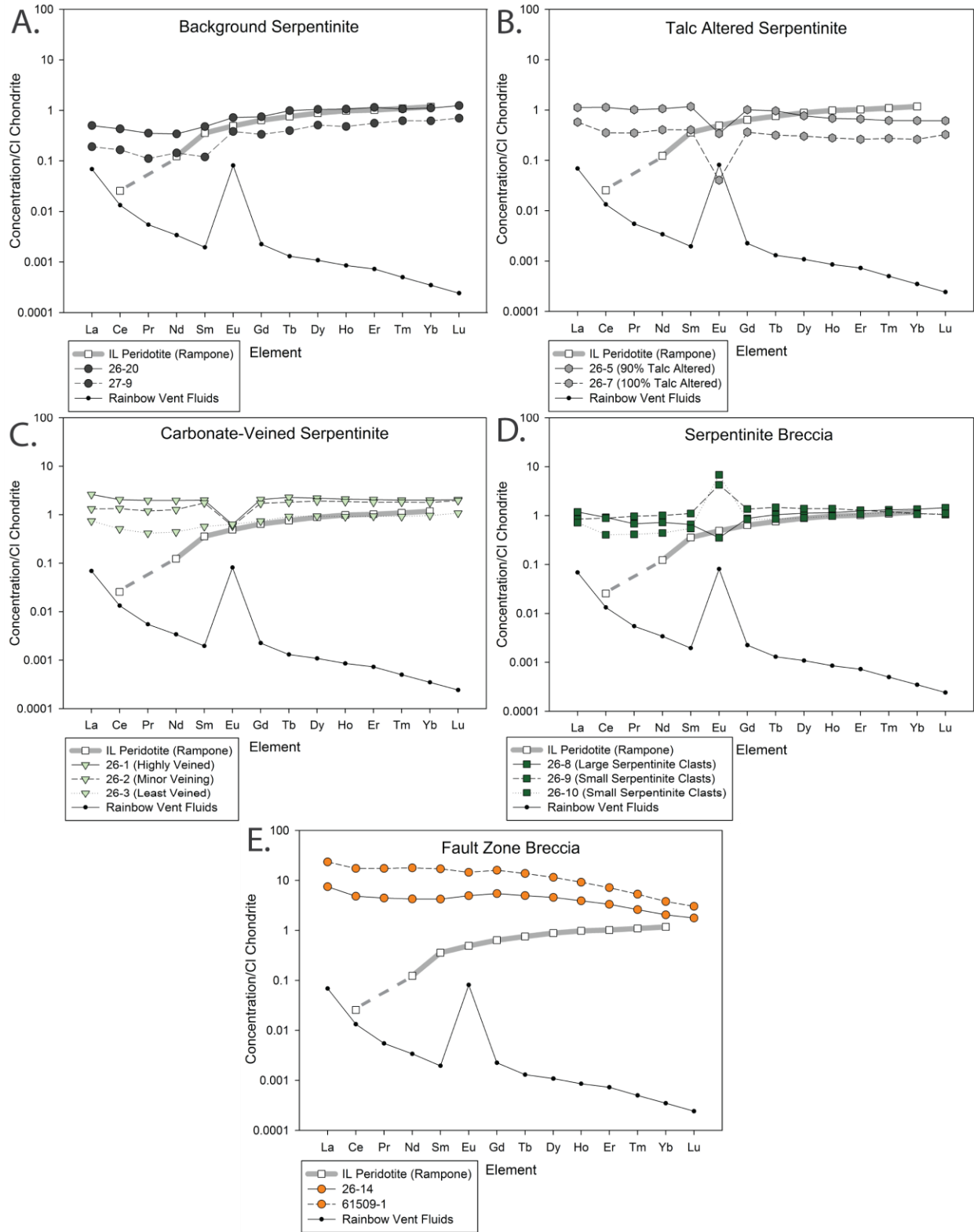


**Figure 8.** Bulk rock major element concentrations of Reppia samples in  $\text{MgO}/\text{SiO}_2$  and  $\text{Al}_2\text{O}_3/\text{SiO}_2$  space.

# Metal Concentrations

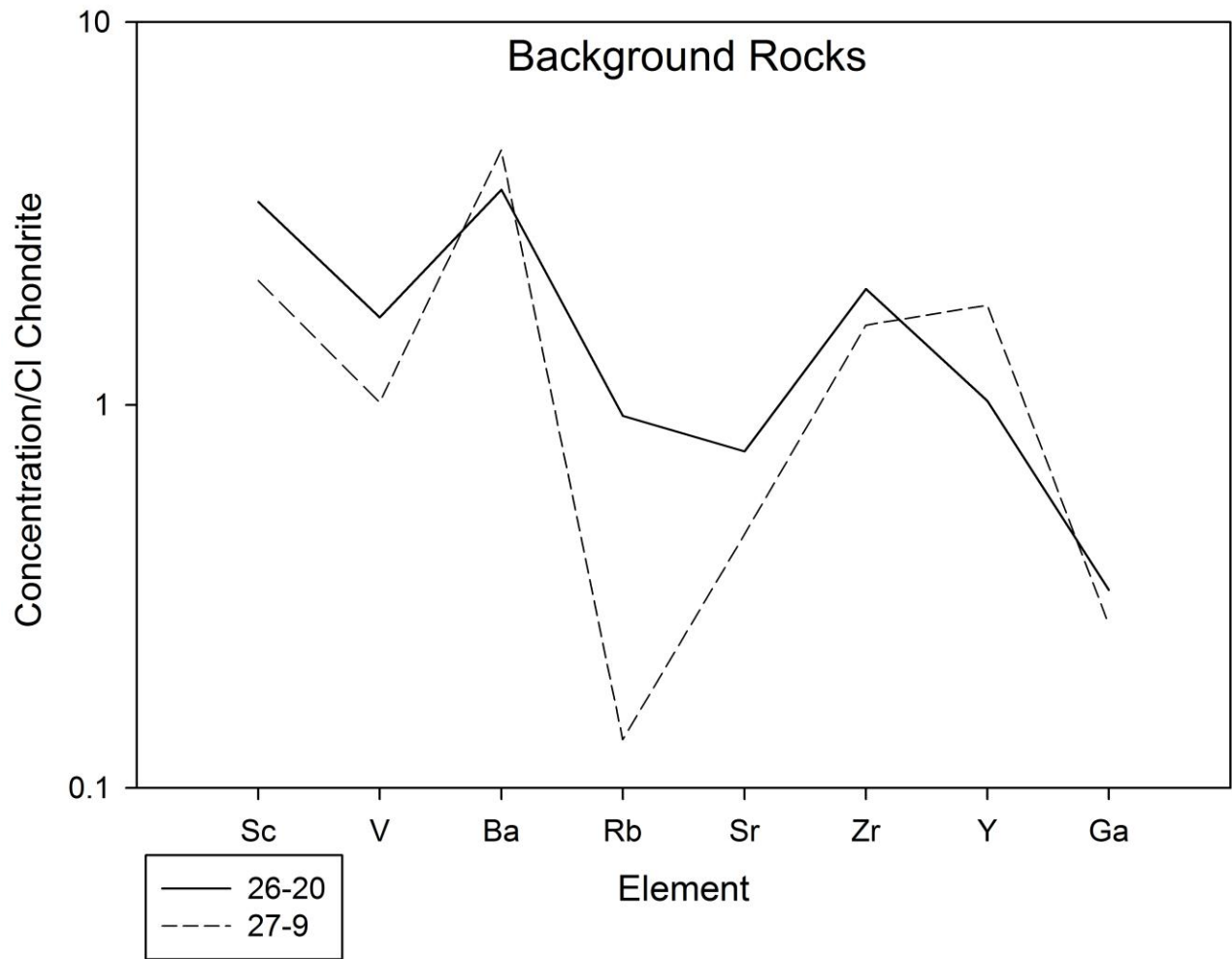


**Figure 9.** Bulk rock metal concentrations of Reppia samples.

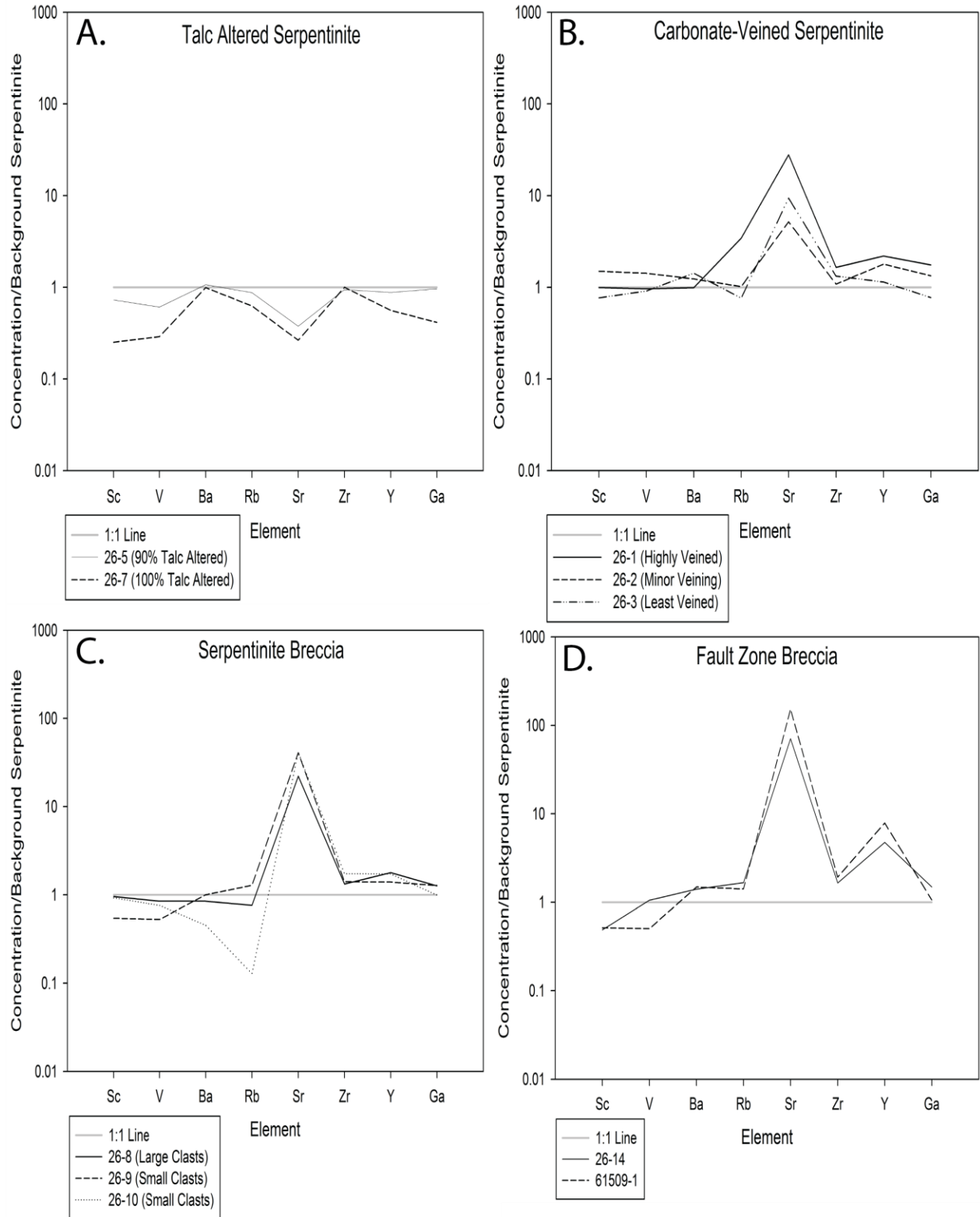


**Figure 10.** Bulk Rock REE Patterns – **A.** Background Serpentinites. **B.** Talc Altered Serpentinites, **C.** Carbonate-Veined Serpentinite, **D.** Serpentinite Breccia, **E.** Fault Zone Breccia. Data for Rainbow hydrothermal fluids patterns from Douville et al., 2002

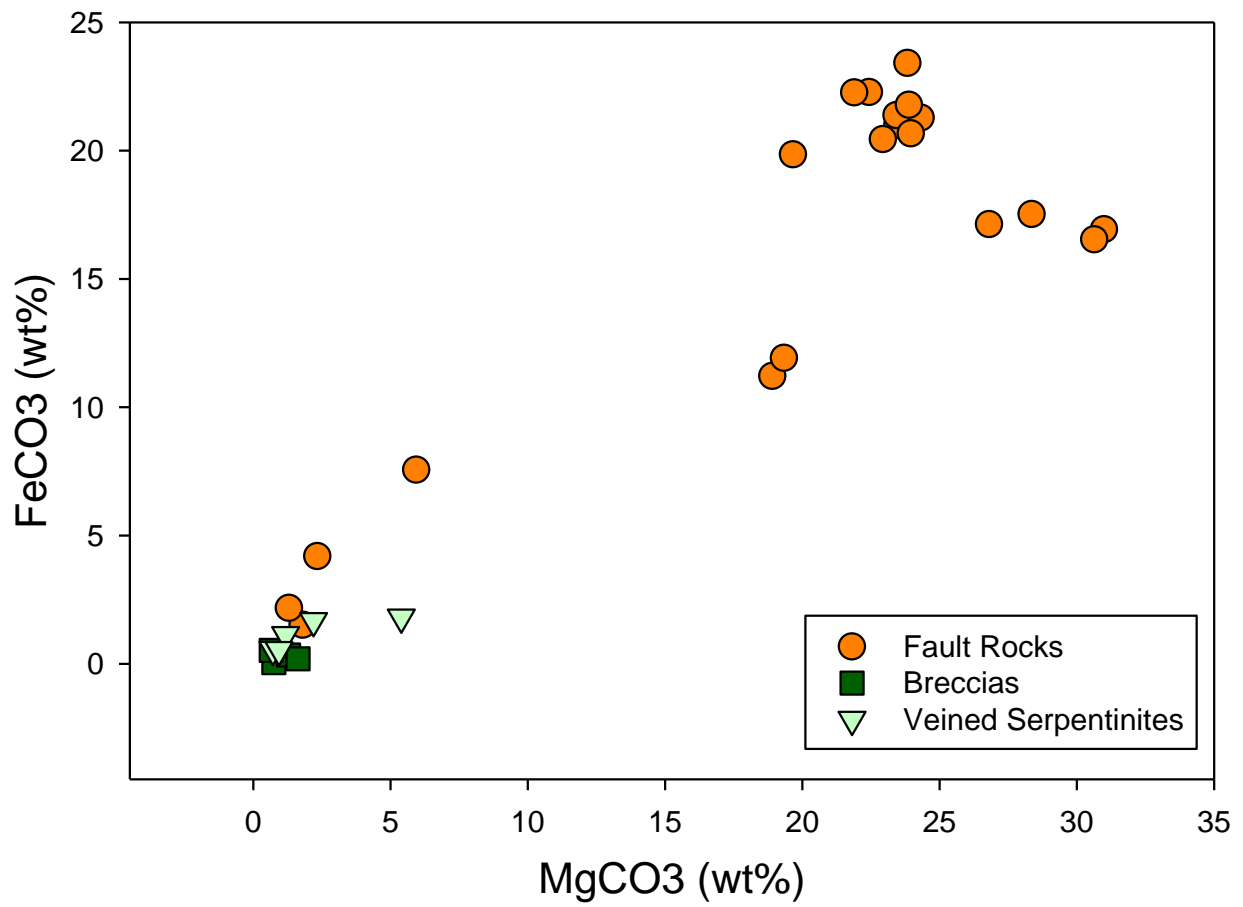




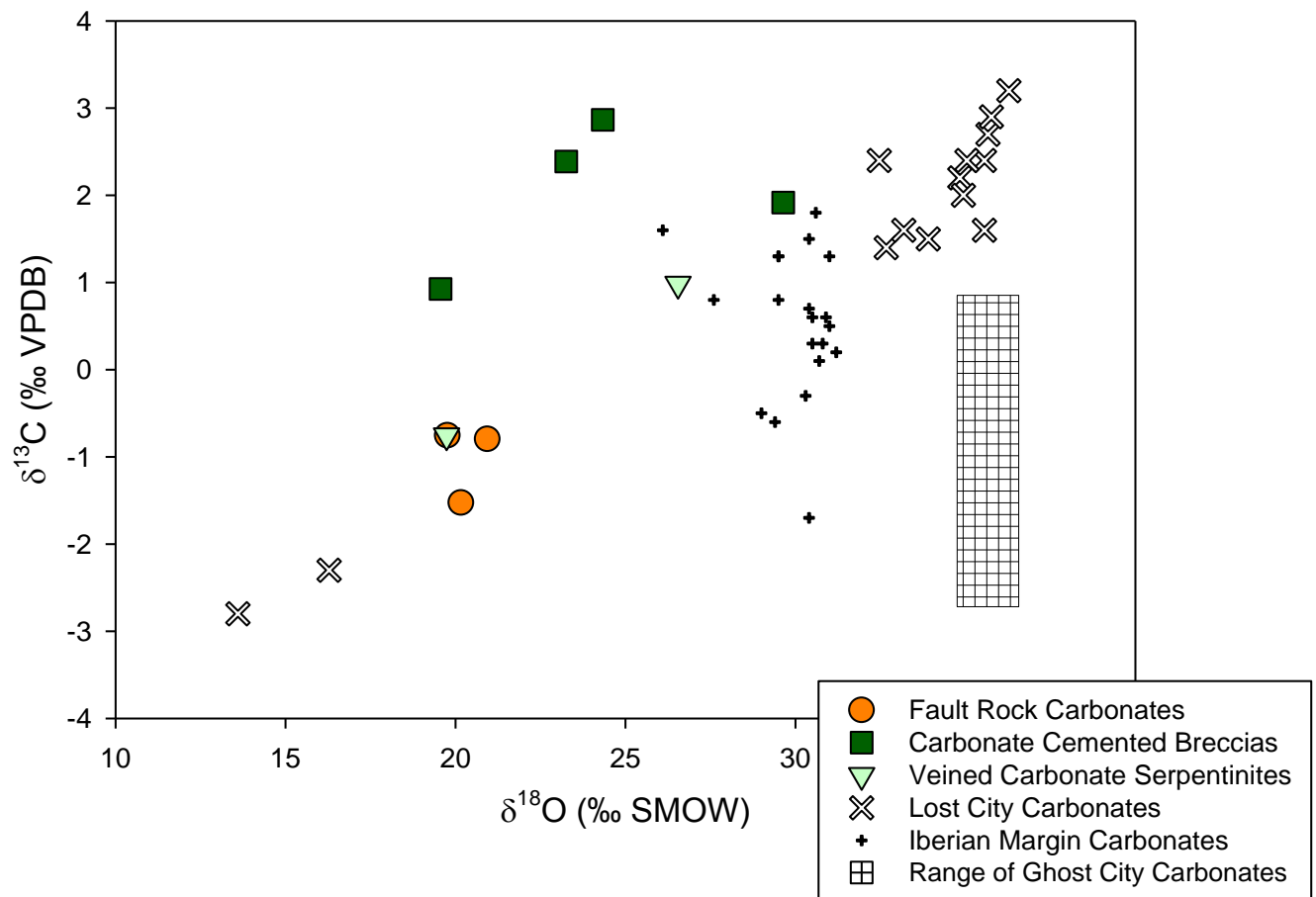
**Figure 11.** Bulk rock trace element analysis of background serpentinites normalized to CI chondrite compositions.



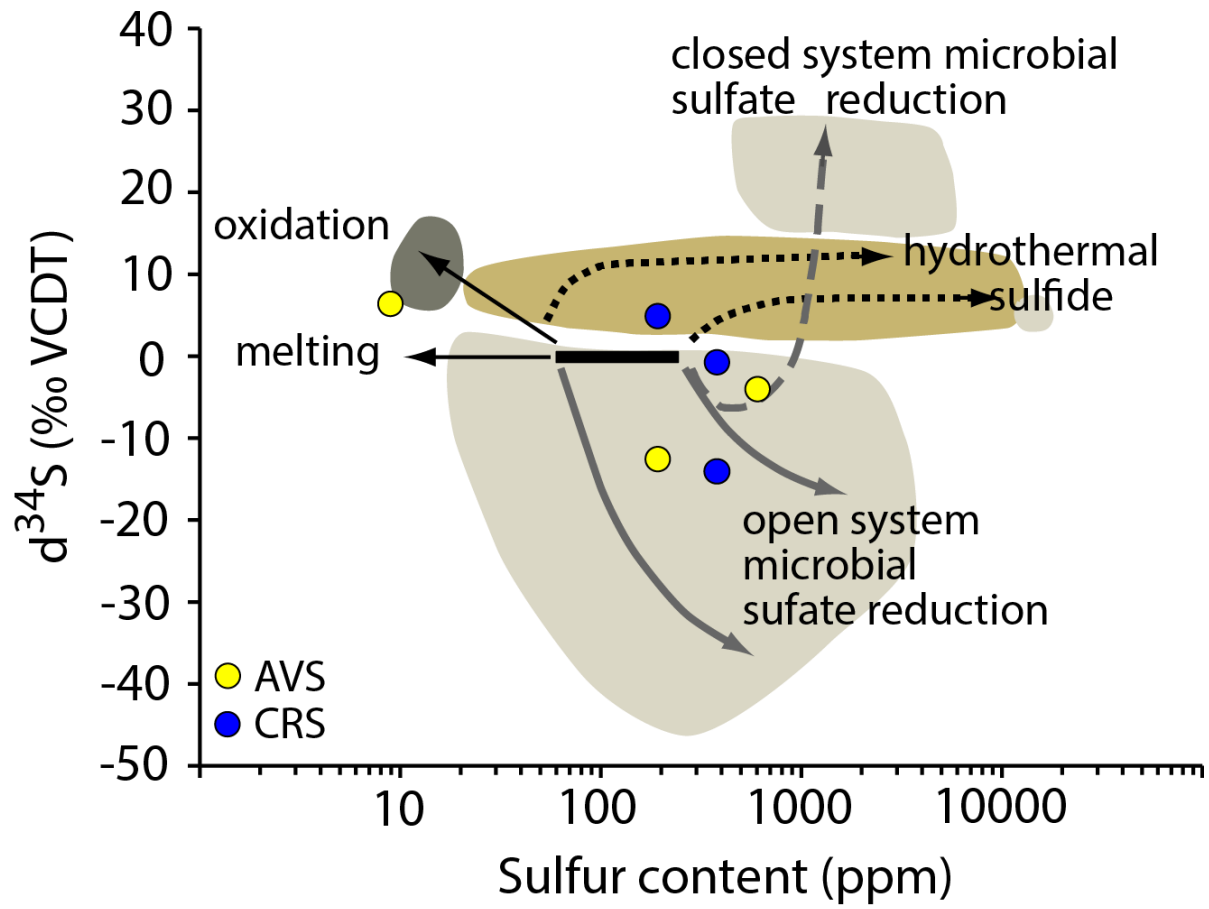
**Figure 12.** Bulk rock trace element analysis of Reppia sample concentrations normalized to background serpentinites. **A.** Talc Altered Serpentinite, **B.** Carbonate-Veined Serpentinite, **C.** Serpentinite Breccia, **D.** Fault Zone Breccia.



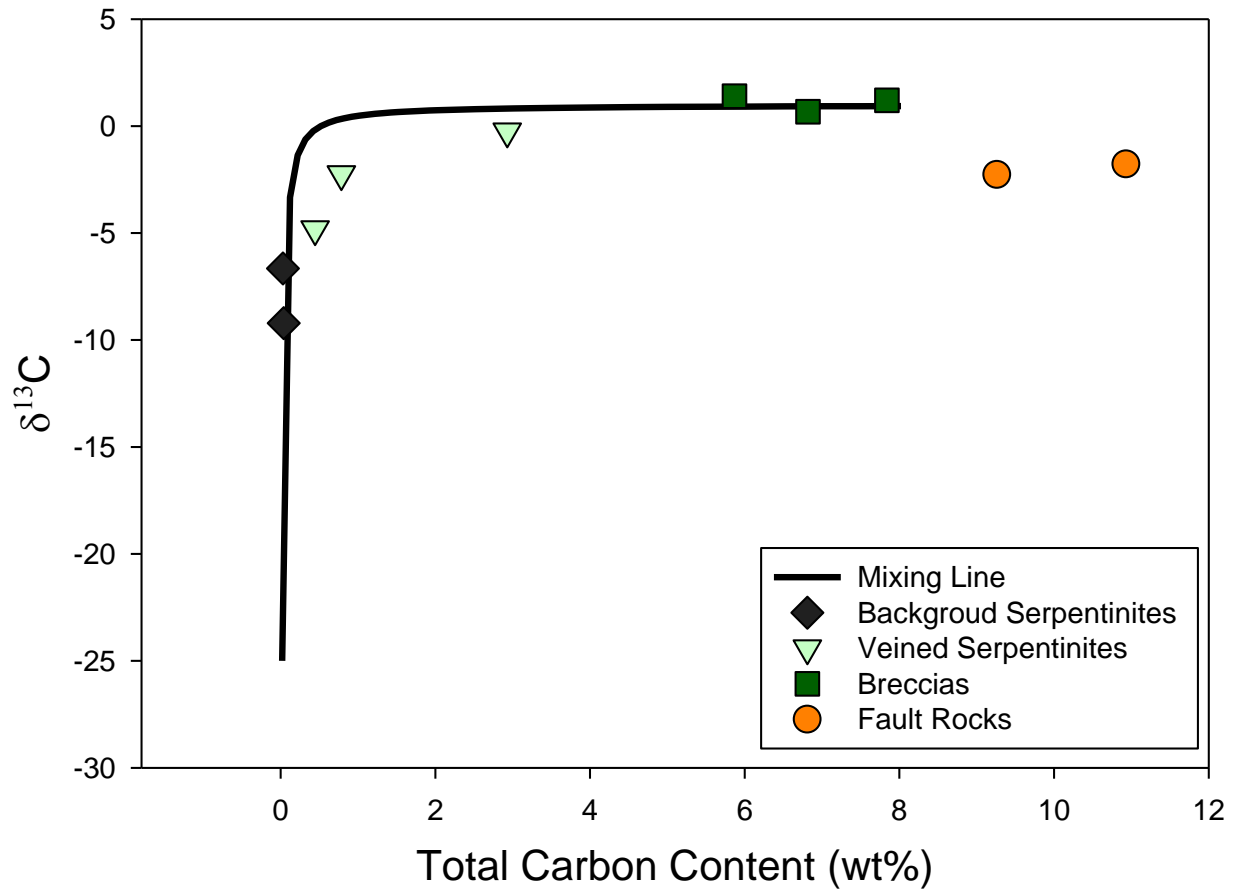
**Figure 13.** Electron probe microanalyzer (EPMA) data for carbonate minerals in various Reppia samples.



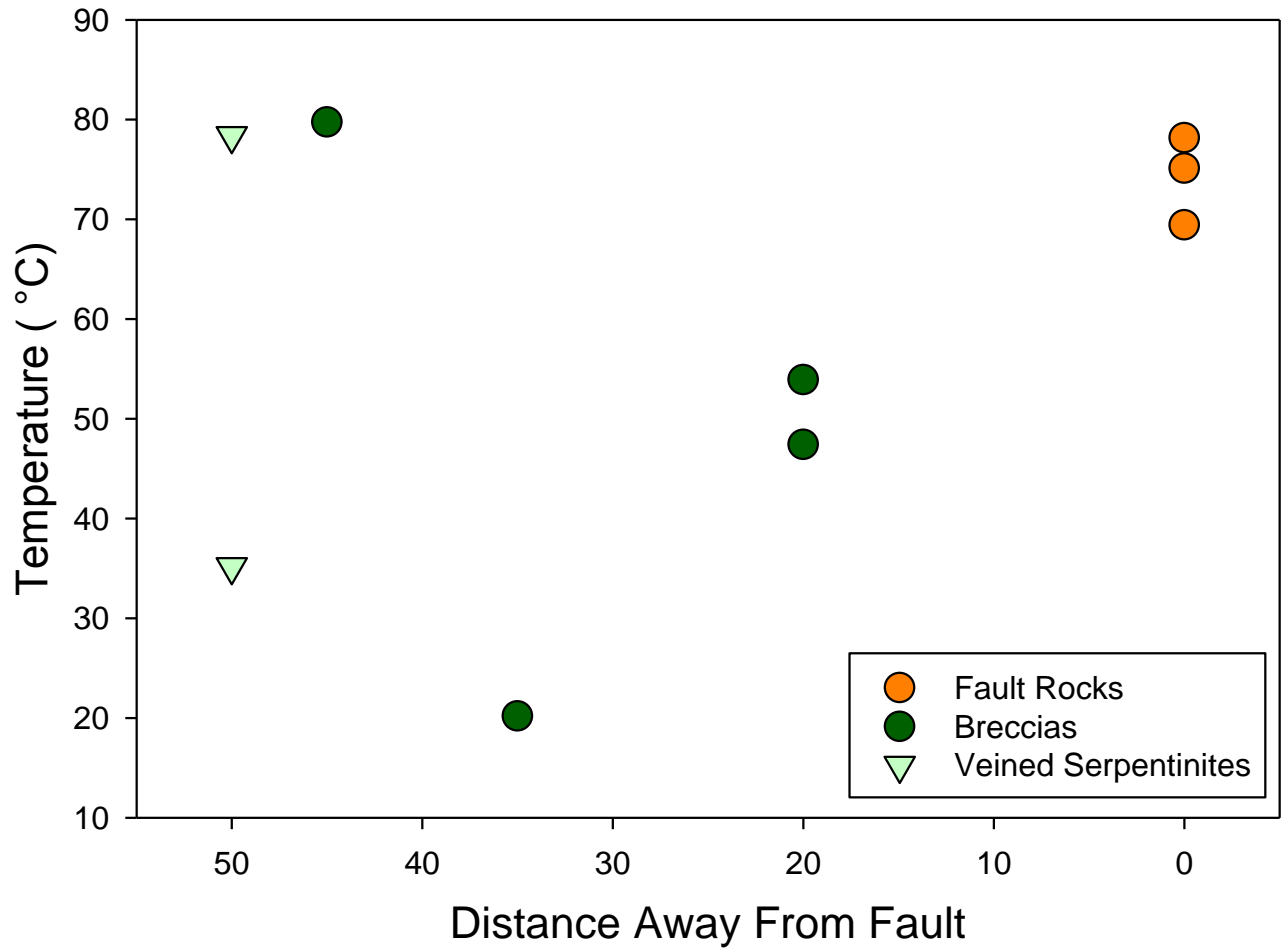
**Figure 14.** Carbon and oxygen stable isotope data of mineral separates from Reppia samples and seafloor UM systems. (data from Lost City, Ghost City, and Iberian Margin respectively from Fruh-Green et al., 2003, Lautuad et al., 2011, Schwarzenbach et al., 2013).



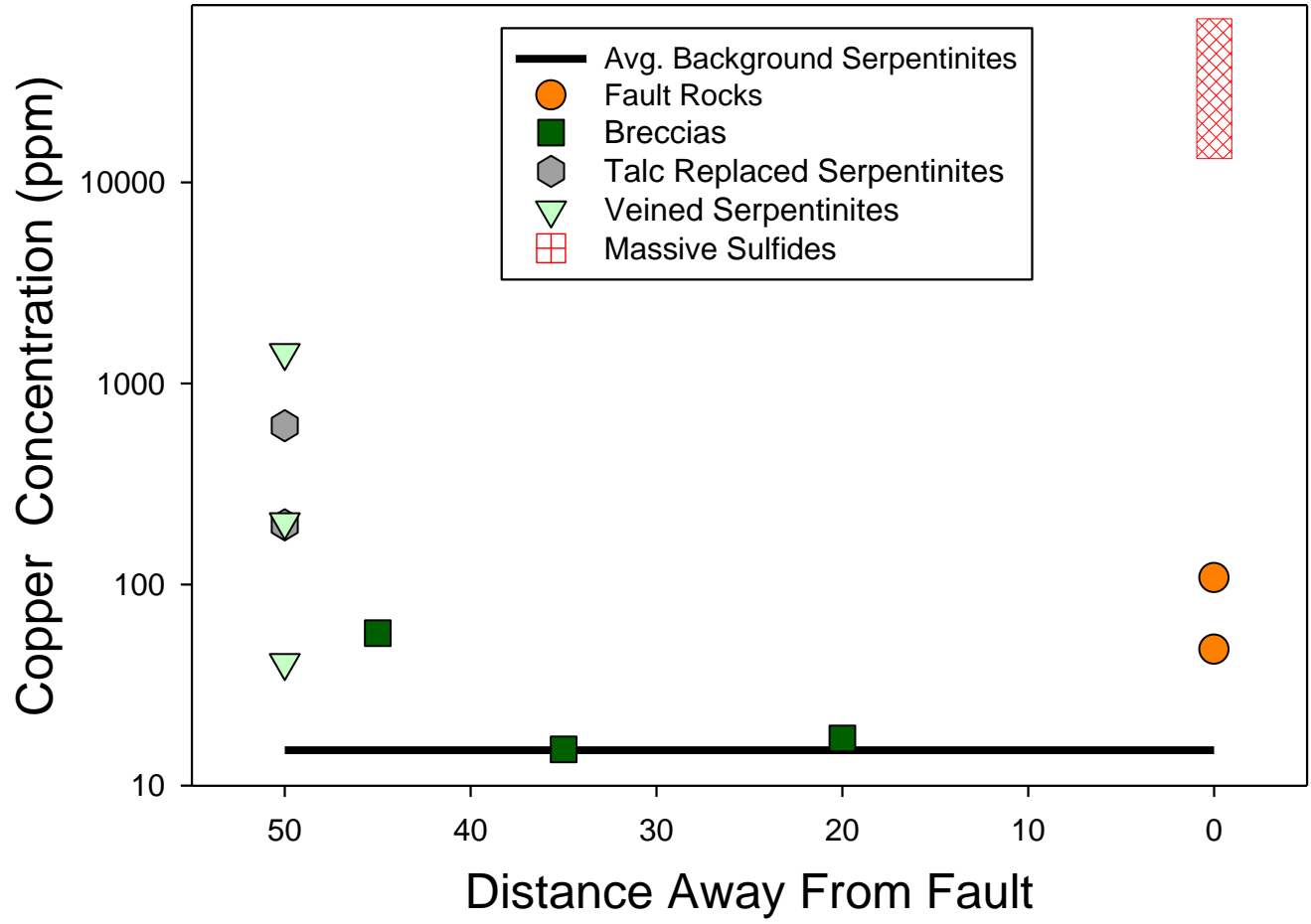
**Figure 15.** Bulk rock  $\delta^{34}\text{S}$  vs sulfur content of serpentinites. Data from Reppia plotted as yellow and blue dots. Sulfur reservoirs are shown by shaded regions and arrows show sulfur pathways. (adapted from Alt et al., 2012).



**Figure 16.** Bulk rock  $\delta^{13}\text{C}$  vs total carbon content for serpentinites. Data plot along a mixing line between seawater carbonate ( $\delta^{13}\text{C}=0\text{‰}$ ) and a low- $\delta^{13}\text{C}$  reduced carbon component ( $\delta^{13}\text{C}=-25\text{‰}$ ). Samples from Reppia plot on this line. (mixing line from Alt et al., 2013)



**Figure 17.** Carbonate temperatures from oxygen isotopes plotted as distance away from fault.



**Figure 18.** Bulk rock copper concentrations plotted as distance away from fault. Data for massive sulfides from Zaccarini and Garuti 2008.



## Tables

	26-1	26-2	26-3	26-5	26-7	26-8	26-9	26-10	26-14	61509-1	26-20	27-9
Normalized Major Elements (Weight %)												
SiO <sub>2</sub>	41.81	46.24	45.18	57.58	62.24	33.61	28.81	24.38	33.74	17.72	46.50	45.58
TiO <sub>2</sub>	0.056	0.065	0.051	0.051	0.010	0.051	0.034	0.039	0.025	0.047	0.055	0.028
Al <sub>2</sub> O <sub>3</sub>	1.83	2.75	1.86	1.44	0.36	1.97	1.10	1.93	1.62	1.43	2.56	1.38
FeO*	10.36	11.38	11.32	11.26	9.48	6.86	5.45	5.05	14.33	9.99	8.62	8.58
MnO	0.056	0.046	0.039	0.017	0.023	0.073	0.244	0.137	0.840	0.826	0.137	0.084
MgO	29.18	37.50	37.85	29.64	27.86	21.00	19.08	13.82	13.60	9.33	40.87	44.31
CaO	16.66	2.01	3.69	0.01	0.02	36.41	45.27	54.63	35.83	60.64	1.26	0.04
Na <sub>2</sub> O	0.00	0.00	0.00	0.00	0.00	0.00	0.00	0.00	0.00	0.00	0.00	0.00
K <sub>2</sub> O	0.04	0.00	0.00	0.00	0.00	0.00	0.00	0.00	0.00	0.00	0.00	0.00
P <sub>2</sub> O <sub>5</sub>	0.003	0.001	0.001	0.001	0.001	0.014	0.010	0.015	0.009	0.008	0.001	0.001
Normalized Trace Elements (ppm)												
NiO	1937.1	3070.3	3189.7	1853.1	530.6	818.1	1579.4	1187.7	1005.3	859.5	2521.7	2833.2
Cr <sub>2</sub> O <sub>3</sub>	3041.2	3952.6	2903.8	2679.7	298.0	2666.9	1783.7	3228.0	2508.5	2336.5	3460.8	2859.9
Sc <sub>2</sub> O <sub>3</sub>	16.2	24.3	12.5	11.9	4.1	15.6	8.8	15.0	8.0	8.4	20.1	12.5
V <sub>2</sub> O <sub>3</sub>	73.1	107.6	68.9	46.2	21.9	64.3	39.9	57.5	79.8	38.2	94.8	56.9
BaO	9.9	12.3	14.2	10.7	9.9	8.5	10.0	4.5	14.0	14.8	8.8	11.2
Rb <sub>2</sub> O	4.2	1.2	0.9	1.1	0.8	0.9	1.6	0.2	2.1	1.7	2.2	0.3
SrO	123.3	22.8	41.4	1.7	1.2	97.8	180.3	183.3	311.6	670.5	5.5	3.3
ZrO <sub>2</sub>	11.4	7.5	9.2	6.5	6.9	9.2	9.7	12.0	11.4	13.3	7.7	6.2
Y <sub>2</sub> O <sub>3</sub>	4.9	4.0	2.5	2.0	1.3	4.0	3.1	3.8	10.6	17.6	1.6	2.9
Nb <sub>2</sub> O <sub>5</sub>	0.0	0.0	0.0	0.0	0.0	0.0	0.0	0.0	0.0	0.0	0.0	0.0
Ga <sub>2</sub> O <sub>3</sub>	4.8	3.6	2.1	2.6	1.1	3.5	3.5	2.7	4.1	2.9	3.0	2.5
CuO	51.1	1780.0	256.7	772.0	248.0	71.7	19.0	21.5	135.2	59.6	19.7	18.1
ZnO	37.0	329.0	137.6	76.4	41.7	39.3	114.2	193.9	84.4	70.7	57.1	48.5
PbO	1.2	0.0	1.2	0.6	1.4	0.2	6.2	1.1	0.0	0.0	0.0	2.1
La <sub>2</sub> O <sub>3</sub>	6.4	0.0	0.0	0.0	0.0	0.0	0.0	1.4	2.5	3.9	0.0	0.0
CeO <sub>2</sub>	6.3	0.0	6.5	4.8	0.0	0.0	0.0	2.5	10.1	19.0	0.7	0.0
ThO <sub>2</sub>	0.0	0.9	0.0	0.3	0.0	0.3	0.3	0.0	0.8	0.8	0.0	0.3
Nd <sub>2</sub> O <sub>3</sub>	1.2	1.7	3.0	4.4	0.7	3.7	0.0	0.0	1.0	12.1	0.0	2.5
U <sub>2</sub> O <sub>3</sub>	1.3	0.2	0.0	1.2	0.0	3.0	0.6	1.0	2.5	0.0	0.0	0.0

**Table 1.** Bulk rock XRF data (normalized).

Carbonate EPMA Compositions												
Sample 61598												
Fault Zone Breccia												
Spot #	2	3	4	5	8	9	10	11				
CaCO <sub>3</sub>	97.14536	96.45073	69.03203	66.47017	53.76315	55.94663	53.82276	53.60698				
MgCO <sub>3</sub>	1.80331	1.300031	18.90934	19.3325	28.35825	26.8047	30.99095	30.63828				
MnCO <sub>3</sub>	1.365045	1.306547	0.747015	2.414269	0.943734	0.896904	0.64266	0.699213				
FeCO <sub>3</sub>	1.518699	2.171298	11.21351	11.91852	17.526	17.13205	16.93242	16.53686				
SrCO <sub>3</sub>	0.132924	0.144606	0.158284	0.175095	0.054851	0.050862	0.032341	0.066248				
Total	101.9653	101.3732	100.0602	100.3105	100.646	100.8311	102.4211	101.5476				
Sample 26-14												
Fault Zone Breccia												
Spot #	1	2	3	4	5	6	7	8	12	13	14	15
CaCO <sub>3</sub>	95.24476	55.20256	52.90324	55.00838	54.63465	55.41477	84.76584	58.91328	56.53757	54.79438	54.68837	54.00373
MgCO <sub>3</sub>	2.337128	23.46813	23.82979	24.31759	23.43361	23.95405	5.939355	19.66467	22.93787	22.43019	21.89157	23.88648
MnCO <sub>3</sub>	0.974523	0.913595	1.07029	1.045821	0.890261	0.998829	1.429375	1.282079	1.082929	0.951675	1.055544	1.057164
FeCO <sub>3</sub>	4.19279	20.98637	23.41035	21.28227	21.37951	20.66805	7.561729	19.8521	20.44229	22.27834	22.26125	21.78264
SrCO <sub>3</sub>	0.358026	0.043881	0.016526	0.089756	0.036757	0.046018	0.17481	0.124946	0.091038	0.069247	0.036187	0.047015
Total	103.1072	100.6145	101.2302	101.7438	100.3748	101.0817	99.87111	99.83707	101.0917	100.5238	99.93291	100.777
Sample 26-10												
Serpentinite Breccia												
Spot #	1	2	3	9								
CaCO <sub>3</sub>	100.7961	100.6262	101.321	99.74255								
MgCO <sub>3</sub>	0.748224	1.279532	0.653676	1.630112								
MnCO <sub>3</sub>	0.01345	0.042617	0.024306	0.029168								
FeCO <sub>3</sub>	0.04757	0.341861	0.522789	0.198989								
SrCO <sub>3</sub>	0.039749	0.028494	0.055278	0.053711								
Total	101.6451	102.3187	102.5771	101.6545								
Sample 26-1												
Carbonate-Veined Serpentinite												
Spot #	3	4	5	8	14							
CaCO <sub>3</sub>	96.04023	95.75716	95.96188	93.17853	93.07091							
MgCO <sub>3</sub>	0.714965	1.177872	0.933345	2.19426	5.392777							
MnCO <sub>3</sub>	0.24436	0.057687	0.236906	0.226859	0.234961							
FeCO <sub>3</sub>	0.555846	1.133945	0.548589	1.677374	1.815086							
SrCO <sub>3</sub>	0.096452	0.088189	0.09232	0.066961	0.125658							
Total	97.65185	98.21486	97.77304	97.34398	100.6394							

**Table 2.** Carbonate EPMA compositions. Analyses that fell outside of  $100 \pm 3.11$  were invalid and not included.

Bulk rock total carbon and isotope composition					
Sample Name	Location		Rock Type	Total Carbon (wt%)	$\delta^{13}C$
	N	E			
26-20	44.3847	9.46233	Background Serpentinite	0.030	-6.66
27-9	44.3831	9.46106	Background Serpentinite	0.040	-9.21
26-2	44.3866	9.45568	Carbonate-Veined Serpentinite	0.445	-4.82
26-3	44.3866	9.45569	Carbonate-Veined Serpentinite	0.784	-2.25
26-1	44.3866	9.45566	Carbonate-Veined Serpentinite	2.930	-0.24
26-8	44.3866	9.4558	Serpentinite Breccia	5.868	1.40
26-9	44.3865	9.45594	Serpentinite Breccia	6.818	0.67
26-10	44.3865	9.45607	Serpentinite Breccia	7.838	1.20
61509-1	44.3866	9.45644	Fault Zone Breccia	9.26	-2.270
26-14	44.3866	9.45642	Fault Zone Breccia	10.93	-1.776

**Table 3.** Bulk rock total carbon and carbon isotopic composition.

Distance from Fault	Sample Name	Location		Rock Type	Analyzed Part	Mineral	$\delta^{13C}$	$\delta^{18O}$	O'Neil (1977)	O'Neil (1977)	Vasconcelos (2005)	Vasconcelos (2005)
		N	E						fluid = 0‰	fluid = +2‰	fluid = 0‰	fluid = +2‰
							VPDB	VSMOW	T(°C)	T(°C)	T(°C)	T(°C)
0	61509-1	44.3866	9.45644	Fault Zone Breccia	Matrix	Dolomite	-0.79	20.94	69.429943	84.7367675	91.21485003	110.1758753
0	26-14-A	44.3866	9.45642	Fault Zone Breccia	Matrix	Dolomite	-1.53	20.16	75.1107676	91.2309621	98.20535878	118.3442261
0	26-14-B	44.3866	9.45642	Fault Zone Breccia	Matrix	Dolomite	-0.75	19.76	78.1641751	94.7340438	101.9851344	122.7823557
20	26-10-A	44.3865	9.45607	Serpentinite Breccia	Matrix	Calcite	2.87	24.33	47.4146976	59.8428774		
20	26-10-B	44.3865	9.45607	Serpentinite Breccia	Matrix	Calcite	2.39	23.26	53.9059096	67.1390257		
35	26-9	44.3865	9.45594	Serpentinite Breccia	Matrix	Calcite	1.92	29.64	20.1885057	29.6123289		
45	26-8	44.3866	9.4558	Serpentinite Breccia	Matrix	Calcite	0.93	19.56	79.7399995	96.5454067		
50	26-1-A	44.3866	9.45566	Carbonate-Veined Serpentine	Vein	Calcite	-0.76	19.74	78.3719957	94.9727917		
50	26-2	44.3866	9.45568	Carbonate-Veined Serpentine	Vein	Calcite	0.98	26.55	35.160045	46.1636782		

**Table 4.** Carbon & oxygen stable isotope compositions of mineral separates and calculated temperatures.

Sample	Rock Type	AVS ppm	$\delta^{34}\text{S}$ AVS (‰)	CRS ppm	$\delta^{34}\text{S}$ CRS (‰)	SO4 ppm	$\delta^{34}\text{S}$ SO4 (‰)	Total S ppm	SO4/Total	$\delta^{34}\text{S}$ Cp (‰)
26-1	Veined Serp.	633.65	-4.1	481.52	-1.4	39.77		1154.9	0.0344	
26-9	Serp. Breccia	202.67	-13.4	364.25	-16.5	55.27	-17.6	622.2	0.0888	
27-9	Bkgd. Serp.	9.67	5.2	201.92	3.9	102.38	4.5	313.97	0.3261	
62712-10	Sulfide Boulder									5.7

**Table 5.** Sulfur concentrations and isotopic signatures.